Tectonophysics 576–577 (2012) 116–132

Contents lists available at SciVerse ScienceDirect

Tectonophysics

journal homepage: www.elsevier.com/locate/tecto

Impact of fracture stratigraphy on the paleo-hydrogeology of the Madison Limestone in two basement-involved folds in the Bighorn basin, (Wyoming, USA)

Mickael Barbier [a,b,*], Rémi Leprêtre [a,c], Jean-Paul Callot [d], Marta Gasparrini [a], Jean-Marc Daniel [a], Youri Hamon [a], Olivier Lacombe [c], Marc Floquet [b]

[a] IFPEN; 1-4 avenue de Bois Préau, Rueil-Malmaison, 92852, France
[b] UP, LGSC EA4234, F-13331 Marseille, France
[c] ISTeP, UMR 7193 UPMC and CNRS, F-75005, Paris, France
[d] LFC-R, UPPA, I.P.R.A. Avenue de l'Université BP 1155, Pau 64013 Cedex, France

ARTICLE INFO

Article history:
Received 22 November 2011
Received in revised form 18 June 2012
Accepted 27 June 2012
Available online 4 July 2012

Keywords:
Fluids
Veins
Fold
Paleohydrogeology
Sheep Mountain
Rattlesnake Mountain

ABSTRACT

Based on the study of the Madison Limestone at Sheep Mountain and Rattlesnake Mountain, a unique outcrop dataset including (1) facies and diagenetic analyses, (2) vertical persistence and cement stratigraphy of vein sets and (3) fluid inclusions thermometry are used to demonstrate the impact of folding and fracturing on paleo-hydrogeology. Quantification of the vertical persistence of fractures shows that Sheep Mountain and Rattlesnake Mountain differ by the vertical persistence of the pre-folding Laramide vein sets, which are strictly bed-confined in Sheep Mountain but cut across bedding at Rattlesnake Mountain, whereas the syn-folding veins are through-going in both. The emplacement chronology and the various sources of the fluids responsible for the paragenetic sequence are based on isotope chemistry and fluid inclusions analysis of the matrix and vein cements. At Sheep Mountain and Rattlesnake Mountain, the cements related to the burial are characterized by isotopic signatures of marine formation waters that were diluted during the karstification of the Madison Platform at the end of Mississippian. Meteoric fluids, presumably migrating during the Cenomanian from Wind River Range and Teton Range, recharge zones located in the south-west of the Bighorn Basin, were remobilized in the early bed-confined and through-going syn-folding veins of the Sheep Mountain Anticline. The former vein set drained only local fluids whose isotopic signature relates to an increase of temperature of the meteoric fluids during their migration, whereas the latter set allowed quick drainage of basinal fluids.

1. Introduction

The characterization of fractured carbonate reservoirs aims at identifying potential fluid flow and hydrocarbon migration pathways, which is an issue considering the high degree of heterogeneity at various scales from the pore to the field. Fractures are the most effective mechanism of reservoir damage at low effective confining pressure, and deeply impact the subsurface oil and gas reservoir properties. Because subsurface data such as cores, well and image logs do not provide enough information to properly characterize the fracture network geometry or connectivity (*e.g.* Angerer et al., 2003; Lynn, 2004a, 2004b) analogue outcrop studies are essential (Ahmadahdi et al., 2008; Barbier et al., 2012a, 2012b; Beaudoin et al., 2011; Fischer et al., 2009; Gross, 1993; Gross et al., 1995; Hanks et al., 1997; Katz et al., 2006; Lacombe et al., 2011; Travé et al., 2000; Wennberg et al., 2006, 2007).

The role of folding, layering, and rock properties on fracture development has been extensively studied in the past few years in order to understand the factors that control the geometry of fracture networks. Following early works (Stearns and Friedman, 1972), several authors have developed a conceptual model relating to folding and fracturing (*e.g.* Bergbauer and Pollard, 2004; Hennings et al., 2000; Price and Cosgrove, 1990), some of which include the role of the pre-existing fractures and faults in perturbing the stress field at local (Bergbauer and Pollard, 2004; Guiton et al., 2003; Sassi et al., 2012) or large scales (Chester, 2003; Savage and Cooke, 2004). The understanding of the controls exerted on the vein network by the distribution of mechanical properties as well as stratigraphic interface properties has made significant progress (*e.g.* Barbier et al., 2012a; Laubach et al., 2009). The concept of stratigraphic control on fracturing has been applied to opening-mode fractures (mode I) and it is now well established that such fractures influence diagenetic history and the hydraulic behavior of strata (Cooke et al., 2006; Fischer et al., 2009; Gross et al., 1995; Lorenz et al., 2002; Shackleton et al., 2005; Wennberg et al., 2006). A clear distinction is now made between the mechanical stratigraphy, which describes sedimentary beds as successive units characterized

* Corresponding author at: TOTAL, CSTJF, BA2010, Avenue Larribau, 64018 Pau, France. Tel.: +33 7 61 71 70 32.
E-mail address: mickael.barbier@total.com (M. Barbier).

0040-1951/$ – see front matter © 2012 Elsevier B.V. All rights reserved.
doi:10.1016/j.tecto.2012.06.048

by mechanical properties, and the fracture stratigraphy which subdivides sedimentary beds into fracturing units according to the fracture network geometry (*e.g.* Barbier, 2012; Barbier et al., 2012a; Laubach et al., 2009). Mechanical stratigraphy is the by-product of depositional composition and structure, associated to chemical and mechanical changes superimposed on rocks after deposition. Together, they considerably influence fracture occurrences, dimensions, vertical persistence and scaling relationships (Gross et al., 1995; Olson et al., 2007; Shackleton et al., 2005).

The fracture network has in turn a key role in constraining the fluid pathways. Mixed marine and meteoric (i.e.. formational), or hydrothermal fluids are associated to cement development, which is affected by the various interactions with host rocks during fluid migration (*e.g.* Beaudoin et al., 2011; Bussolotto et al., 2007; Dietrich et al., 1983; Fischer et al., 2009; Lefticariu et al., 2005). Fluid rock interaction within fault zones has been the focus of several studies (*e.g.* Templeton et al., 1995; Travé et al., 2000, 2007). Similarly, several authors already focused on the migration of meteoric water invading sedimentary cover detached in fold and thrust belts (*e.g.* Evans and Hobbs, 2003). Nevertheless, though the role of the initial sedimentary facies on the diagenetic evolution and subsequent fracturing pattern has been described (*e.g.* Barbier et al., 2012a; Wennberg et al., 2006), only few attempts have been made to combine the fracture infill type with the structural evolution of the fracture network to produce a description of the fluid pathways through time during folding (Beaudoin et al., 2011; Fischer et al., 2009; Travé et al., 2000).

The aim of this paper is to understand the rock–fluid interaction and its evolution during fold development. For this purpose, new geochemical and fluid inclusion analyses were added to the fracture stratigraphy study proposed by Barbier et al. (2012a). These analyses were carried out on a world-class analogue of fractured carbonate reservoir, the Madison Limestone (Wyoming) at Sheep Mountain anticline (Barbier et al., 2012a, 2012b; Beaudoin et al., 2011; Katz et al., 2006; Reid et al., 1993; Smith et al., 2004; Westphal et al., 2004) and at Rattlesnake Mountain anticline (Beaudoin et al., 2012–this issue; Neely and Erslev, 2009). This study is based firstly on existing results on (1) the fracture network orientation (*e.g.* Amrouch et al., 2010; Barbier et al., 2012a; Beaudoin et al., 2011; Bellahsen et al., 2006a), (2) vertical persistence and spatial ordering of the fracture network (Barbier et al., 2012a), (3) the diagenetic evolution of the Madison Limestone (Barbier, 2012; Barbier et al., 2012b), and secondly on new observations, including fluid inclusion analyses (complementing those of Katz et al., 2006 and Beaudoin et al., 2011). The integration of those results is necessary to constrain the evolution of mechanical properties during diagenesis, and determine how this evolution controls the distribution and evolution of fluid and ultimately the hydrogeology of the folds.

2. Geological setting

2.1. Regional setting

The Madison Limestone crops out at several localities in Wyoming, including Sheep Mountain and Rattlesnake Mountain (Fig. 1). Sheep Mountain and Rattlesnake Mountain are both basement arches developed during the Eocene thick-skinned Laramide Orogeny in the western U.S. (Erslev, 1990; Neely and Erslev, 2009). The two structures are interpreted to have formed under a mean N065 compressional stress trend (Amrouch et al., 2010; Beaudoin et al., 2012–this issue; Craddock and Van der Pluijm, 1999; Neely and Erslev, 2009).

Sheep Mountain is a doubly plunging, asymmetric, 16 km long and 2 km wide east-verging structure with a NW–SE orientation (Fig. 2A; Amrouch et al., 2010; Bellahsen et al., 2006a). The fold provides excellent outcrops of the Madison Limestone and is located close to the Spence dome oil field, on the eastern flank of the Bighorn Basin (Stanton and Erslev, 2004).

Rattlesnake Mountain, located in the eastern flank of the Bighorn Basin, is a 35 km long and 8 km wide, west verging structure with a

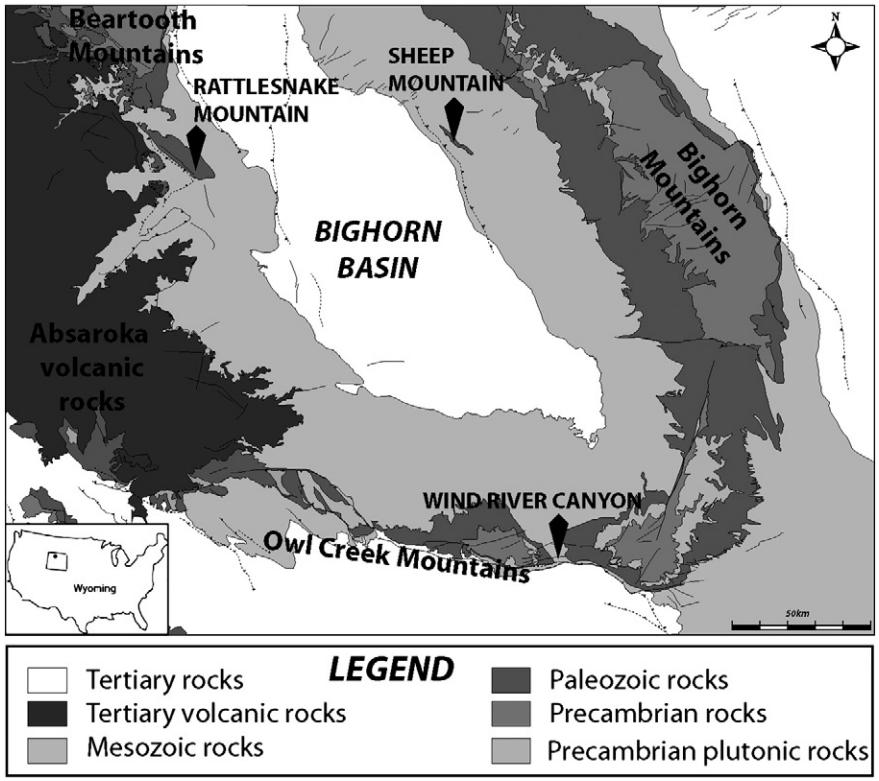

Fig. 1. Location of the studied area: Geological map of the Bighorn Basin, with a cross section of the Bighorn basin running from the Wind river Basin to the Bighorn Mountain (from Beaudoin et al., 2012–this issue).

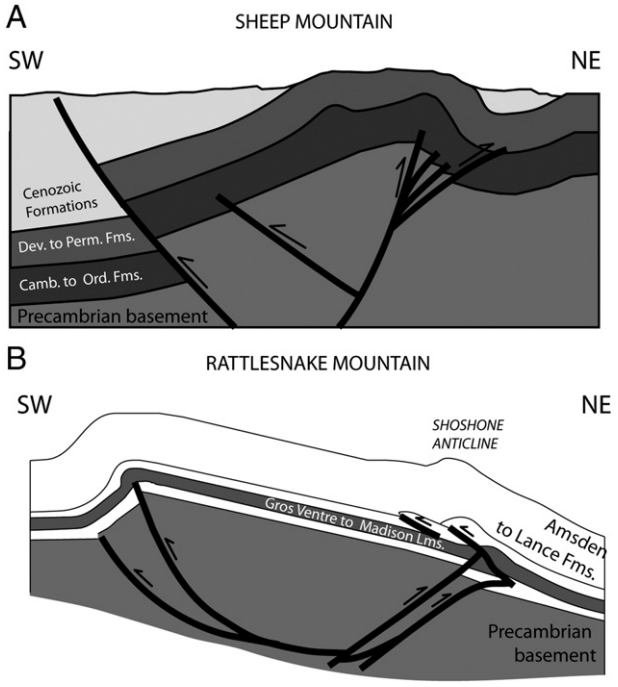

Fig. 2. A) Cross sections of Sheep Mountain (modified from Amrouch et al., 2010), and B) Rattlesnake Mountain (modified from Neely and Erslev, 2009; see also Beaudoin et al., 2012–this issue).

NW–SE orientation (Fig. 2B; Neely and Erslev, 2009). This fold is cored by Precambrian gneiss thrusted onto the Flathead and Bighorn Formations (Cambrian and Ordovician respectively). To explain the sedimentary cover geometries, Erslev (1990) proposed that the shortening event was accommodated during Laramide times with little penetrative strain in the basement rocks and rigid block rotation (Erslev, 1991, 1995; Neely and Erslev, 2009; Stearns, 1971). Beaudoin et al. (2012–this issue) offer an alternative interpretation of Rattlesnake Mountain, with a fault zone more distributed, based on the study of fault throw distribution along the major thrusts.

2.2. Fracture sets

Within the two folds, the Madison Limestone shows numerous structures related to the compressive stress regime of both Sevier and Laramide shortening phases (Amrouch et al., 2010, 2011; Beaudoin et al., 2011; Bird, 1998): bed-confined vertical vein sets, bedding-parallel and perpendicular stylolites, through-going veins. Four sets of fractures have been defined at Sheep Mountain based on the set orientations and relative chronology (Bellahsen et al., 2006a, b and detail therein, see Fig. 3). Set I corresponds to bed-confined and through-going calcite veins striking N110–130°E. These veins initiated as joints parallel to the foreland compressive stresses during the Sevier Orogeny (Amrouch et al., 2010), reactivated by shearing during folding (Bellahsen et al., 2006a). Set II, mainly developed in the backlimb (slightly in the hinge) of the fold (Fig. 3), are bed-confined veins, parallel to the shortening direction, during the Eocene Laramide Orogeny. Set III comprises both bed-confined and through-going bed-perpendicular veins striking N130°E, and mostly developed in the fold hinge zone (Fig. 3). Accordingly, Set III is considered to have been created during folding in response to strata bending. Set IV comprises vertical veins (oblique related to the bedding) striking N110°E created at the end of the fold exhumation, probably during the stress relaxing stage (Bellahsen et al., 2006a) as they are mainly associated with small normal faults. A similar but more complex fracture network occurs at Rattlesnake Mountain (Beaudoin et al., 2012–this issue). This network comprises a nearly prefolding Sevier-related set composed of two orthogonal families (N–S to N020°E and E–W, and a N110–130°E trending set similar to Set I at Sheep Mountain), followed by the two Laramide-related sets, a N045°E pre-folding Set II, and the N130°E syn-folding Set III. A last post-folding N–S Set is also encountered.

2.3. Stratigraphy and sedimentology

The investigated Mississippian Madison Limestone is composed of six third-order sequences forming a large-scale second order sequence (*e.g.* Barbier, 2012; Barbier et al., 2012b; Sando, 1988; Smith et al., 2004; Sonnenfeld, 1996a, 1996b; Westphal et al., 2004). The bottom two third-order sequences at Sheep Mountain show multiple facies organized into three facies associations which are typical of a

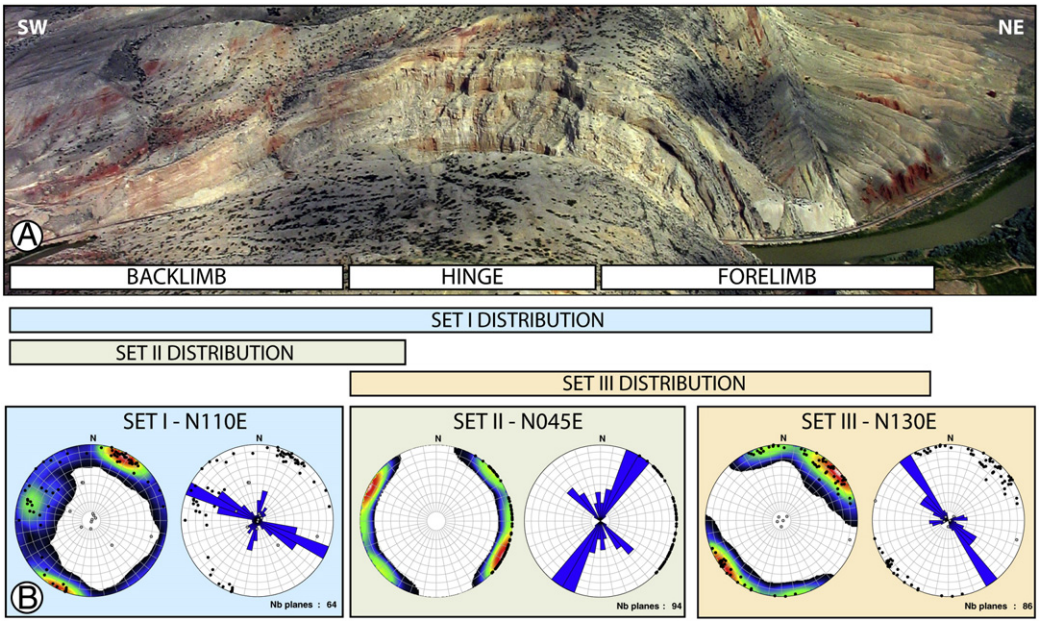

Fig. 3. A) Along strike view of the studied cross section at Sheep Mountain. B) Stereogram and distribution of the analyzed fracture sets at Sheep Mountain, depending on their structural position.

(1) supratidal environment, (2) intertidal environment and (3) storm influenced subtidal environment (*e.g.* Barbier et al., 2012a; Fig. 4). A detailed petrographic study of 270 thin sections (180 for Sheep Mountain and 90 for Rattlesnake Mountain) allowed Barbier et al. (2012a, 2012b) to define the paragenetic sequence of the succession. This study shows that (1) supratidal facies are strongly affected by early dolomitization; (2) oolitic and bioclastic grainstones display early isopachous and syntaxial marine calcite cements followed by mechanical and chemical compaction; and (3) subtidal wackestones and packstones exhibit early syntaxial calcite cement and are partially dolomitized both before and after mechanical compaction.

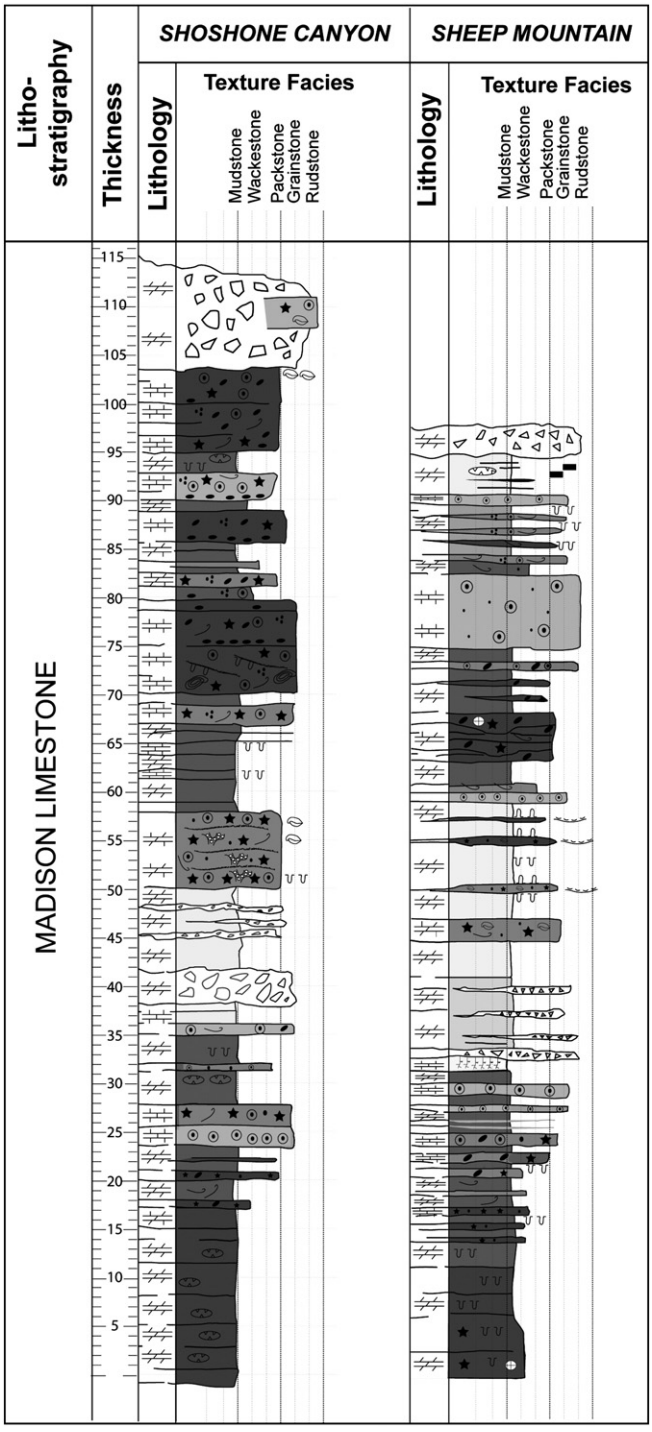

Fig. 4. Sedimentological logs of the Madison Limestone at Shoshone Canyon and Sheep Mountain.

3. Methods and datasets

3.1. Diagenetic and stable isotope datasets

The diagenetic descriptions have been made on two detailed sedimentological sections located at Sheep Mountain and Shoshone Canyon (Fig. 1). Each of these sections has been described at the 1/500 scale (Fig. 3). About 270 thin sections (made from oriented plugs, sampled with a semi systematic method, a sample every meter with specific focus in case of local, small-scale facies variations) were thoroughly analyzed for faciologic and diagenetic purposes. All thin sections have been stained with alizarin red-S and potassium ferricyanide (Dickson, 1966) to differentiate carbonate minerals (aragonite, calcite are stained, while dolomite remains unstained) and distribution of ferrous iron. Petrographic observations included conventional and cathodoluminescence microscopy (Technosyn Cold CL Model 8200 Mark II, Technosyn Corp., Cambridge, MA, USA; operation conditions were 16–20 kV gun potential, 420–600 μA beam current, 0.05 Torr vacuum and 5 mm beam width; and OPEA system, OPEA France; operation conditions 12–14 kV gun potential).

The various diagenetic phases were carefully sampled (using a dentist micro-drill) in order to analyze their carbon and oxygen stable isotopic composition. Carbonate powders were reacted with 100% phosphoric acid (density >1.9, Wachter and Hayes, 1985) at 75 °C using a Kiel III online carbonate preparation line connected to a ThermoFinnigan 252 mass-spectrometer. All values are reported in per mil relative to V-PDB by assigning a $\delta^{13}C$ value of +1.95‰ and a $\delta^{18}O$ value of −2.20‰ to NBS19. Oxygen isotopic compositions of dolomite were corrected using the fractionation factors given by Rosenbaum and Sheppard (1986). Reproducibility was checked by replicated analysis of laboratory standards and is better than ±0.02 (1σ).

3.2. Microthermometry

Six samples from the Madison Limestone at Sheep Mountain have been investigated for fluid inclusion (FI) characterization on thin sections (30 μm) and mirror-like wafers (80–100 μm). The samples can be subdivided into two types: 1) oolitic and crinoidal grainstones hosting isopachous, syntaxial and sparry calcite cements and 2) dolosparite, partially recrystallized and locally dedolomitized. Both sample types may contain one or several sets of fractures, namely Sets I (FN110E), II (FN045E) and III (FN130E).

Fluorescence microscopy and FI microthermometry were done with a Linkam MDS 600 heating–freezing stage, calibrated with synthetic FIs, and mounted on a Nikon LV100 Eclipse, associated to a 100 W Mercury vapor lamp. The Linksys 32 software enabled all the operations for FI microthermometry.

Monophase aqueous FIs were stretched to artificially nucleate a vapor bubble, which allowed ice melting measurements (Tm_i). Oil density was qualitatively estimated from fluorescence color of hydrocarbon FIs based on the conversion chart from McLimans (1987).

The software package FLUIDS (Bakker, 2003, 2009) was used to further characterize the aqueous fluids. Bodnar's (1993) AQSO1 software was used to calculate salinities from Tm_i in the binary H2O–NaCl system. The application BULK was used to calculate bulk fluid properties (*e.g.* density) of individual FIs using the equation of state of Krumgalz et al. (1996). The program LONER32 was used to calculate the isochore slope according to the model of Bodnar and Vityk (1994).

3.3. Fracture datasets

In this study, we mostly rely on this existing chronological setting of the different fracture sets that have been recognized and characterized based on strike and opening mode by Bellahsen et al. (2006a) and Amrouch et al. (2010) at Sheep Mountain and by Barbier (2012) and Beaudoin et al. (2012–this issue) at Rattlesnake

Fig. 5. Outcrop photography of the Lower portion of the Madison Limestone divided into two large-scale fracturing units (FU1) and ten intermediate-scale fracturing units (FU2) (modified from Barbier et al., 2012a, 2012b). Fracture orientation has been controlled by field orientation measured along the outcrop. On the right the synthetic sedimentary log is represented.

Mountain. At the macroscale, we adopt the scan line method for reporting fracture intensity (La Pointe and Hudson, 1985; Wennberg et al., 2006). This method consists of counting the number of fractures per unit length along a sample line oriented perpendicular to each fracture set to reduce the measurement deviation. The spatial variability of the spacing values between fractures were statistically analyzed using moving average trendlines. A cumulative length of more than 2.7 km and 1.5 km of scan lines at Sheep Mountain and Rattlesnake Mountain respectively was carried out, along each sedimentary bed and for each fracture sets observed at both. Morphology, orientation, cross-cutting relationships, texture and nature of fracture filling were recorded for each fracture and each fracture set. Roughly 3400 fractures were measured (2696 at Sheep Mountain and 700 at Rattlesnake Mountain) allowing us to describe at least three hierarchical orders of fracturing units (small-scale, intermediate and large-scale fracturing units; Barbier et al., 2012a). The latter units are defined by stratigraphic surfaces that arrest fracture propagations. They were statistically characterized using the method used by De Keijzer et al. (2007).

4. Fracture network characterization

At Sheep Mountain, large- and intermediate-scale fracturing units (FU1 and FU2) show through-going persistent veins belonging to both Set I and Set III connecting a large part of the third-order depositional sequence (Fig. 5; Barbier et al., 2012a). They are bounded by the most prominent interfaces, located at major sedimentary and/or textural changes, which form important sliding surfaces (Fig. 6; Barbier et al., 2012a; Sanz et al., 2008). Only few fractures of Set II appear to form large-scale connections (Fig. 6). FU1 and FU2 can be subdivided into small-scale fracturing units (FU3) (Figs. 5 and 6). At this scale of fracturing, the three sets are expressed and their distribution is controlled by sedimentary facies, bed thickness and related diagenetic overprint (Barbier et al., 2012a). For instance, small-scale fracturing units correspond to entire facies sequences when no or little petrophysical and mechanical property contrasts between beds are observed (Fig. 7). Conversely, small-scale fracturing units correspond to each bed of a facies sequence in the case of high contrasts of petrophysical and mechanical properties between beds. For instance, all beds of a dolomitized supratidal facies sequences can be considered as a single mechanical unit, whereas each bed of both intertidal and subtidal facies sequences acts as an independent mechanical unit because of a different diagenesis within each beds.

At Rattlesnake Mountain (Fig. 8), fracturing units are thicker than at Sheep Mountain whatever the scale of observation due to three mains reasons (Barbier, 2012): 1) although several sedimentary interfaces are recognized as decoupling slip interfaces, most of the bed interfaces show large stylolitic planes at Rattlesnake Mountain, which increase the degree of coupling between beds and thus the vertical persistence of fractures; 2) the Madison Formation was cemented during burial that homogenized mechanical properties of the stratigraphic column; 3) the Madison Formation at Rattlesnake Mountain was buried deeper than at Sheep Mountain, which also influences the propagation of fractures.

5. Fluid inclusions data

5.1. Fluid inclusion description

Ten different FI types were recognized within seven samples in both matrix and fracture diagenetic mineral phases. The data set is composed of 190 measured inclusions (Table 1) on these seven samples. Fig. 9 schematically represents how these FIs are distributed within the different crystals, and Table 1 summarizes the FI main petrographic features as well as the results of the microthermometric analysis, the latter graphically represented in Fig. 10.

5.1.1. Fluid inclusions in host rock cements

Four types of FI were described in host rock cements. They are observed in syntaxial calcite cements, dolosparites, and sparry calcite cements. Type 1 inclusions are monophase all-liquid aqueous FIs found in syntaxial calcite cements (Fig. 9A). They commonly occur in patches or sometimes isolated. Less commonly, they occur along pseudo-secondary trails (not cross-cutting the whole crystal). Type

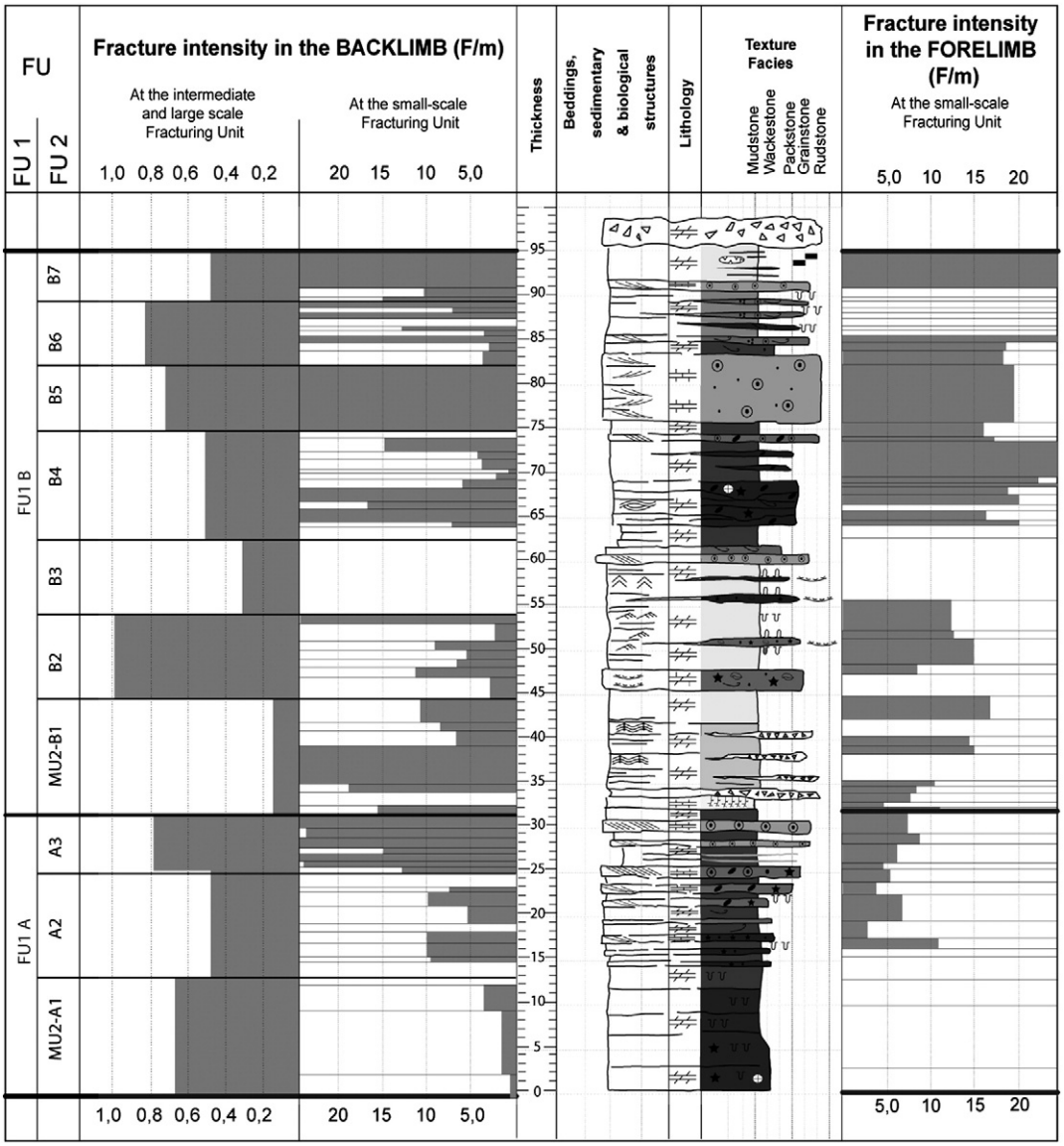

Fig. 6. Fracture stratigraphy of the lower part of the Madison Limestone for both limbs of the Sheep Mountain Anticline. The mean fracture intensity has been measured for each small-scale and intermediate fracturing units. Note the quasi absence of set II fractures at the scale of intermediate fracture units.

2 inclusions are monophase aqueous all-liquid FIs, homogeneously distributed within the dolomite crystal cores, typical of primary FIs (Fig. 9B). They may have shapes controlled by crystallographic directions. Rare leaked Type 1 FIs present vapor bubbles of variable volume. Type 3 inclusions are monophase aqueous all-liquid FIs found in dolomites (Fig. 9B). They are less abundant than Type 2 and randomly distributed within the dolomite clear external rims, with shapes controlled by crystallographic directions, suggesting a primary origin. Type 4 inclusions are monophase all-liquid aqueous FIs observed within the sparry calcite crystals (Fig. 9C). They occur in patches but commonly without any preferential concentration.

5.1.2. Fluid inclusions in Sets I and II veins

Three types of FI were observed in sparry and blocky calcite that healed Sets I and II veins. Type 5 inclusions are monophase all-liquid aqueous FIs in Set I calcite occurring in isolation or in patches, with shapes commonly controlled by crystallographic directions (Fig. 9D). Type 6 inclusions are bi-phase oil-rich FIs located along secondary trails in calcite of Set I veins (Fig. 9D). The oil coexists with a gas bubble (degree of fill on section between 0.6 and 0.8) and is highlighted by a green color under UV-light (30–40 API, after McLimans, 1987). An aqueous phase, suspected to coexist with the hydrocarbon, was not unambiguously observed by optical means. Type 7 inclusions are monophase all-liquid aqueous FIs found in calcite of Set II veins. They exhibit shape and distribution and characteristics like Type 5 FIs within Set I calcite (Fig. 9E).

5.1.3. Fluid inclusions in Set III veins

Three types of FI were observed in blocky calcite cements that healed the Set III veins. Type VIII inclusions are hydrocarbon, biphase oil-rich FIs coexisting with gas bubbles (degree of fill is 0.5 to 0.8) are found in calcite of Set III veins. Their distribution is variable but shapes commonly controlled by crystallography suggest a primary origin (Fig. 9F). The oil has a green fluorescence like Type 6 FIs. The presence of an aqueous liquid is observed in some FIs, mainly in sample SM2.08. The variable oil versus water proportions suggests heterogeneous trapping (Fig. 9F). Type 9 inclusions are monophase all-liquid aqueous FIs coexisting, with the hydrocarbon Type 8 (Fig. 9F), within the calcite crystal cores of Set III veins. Type 10 inclusions are aqueous two-phase liquid-rich FIs, found mainly in patches within calcite of Set III veins. The degree of fill is quite variable (0.6–0.8) FIs with the higher vapor proportion being located near the borders

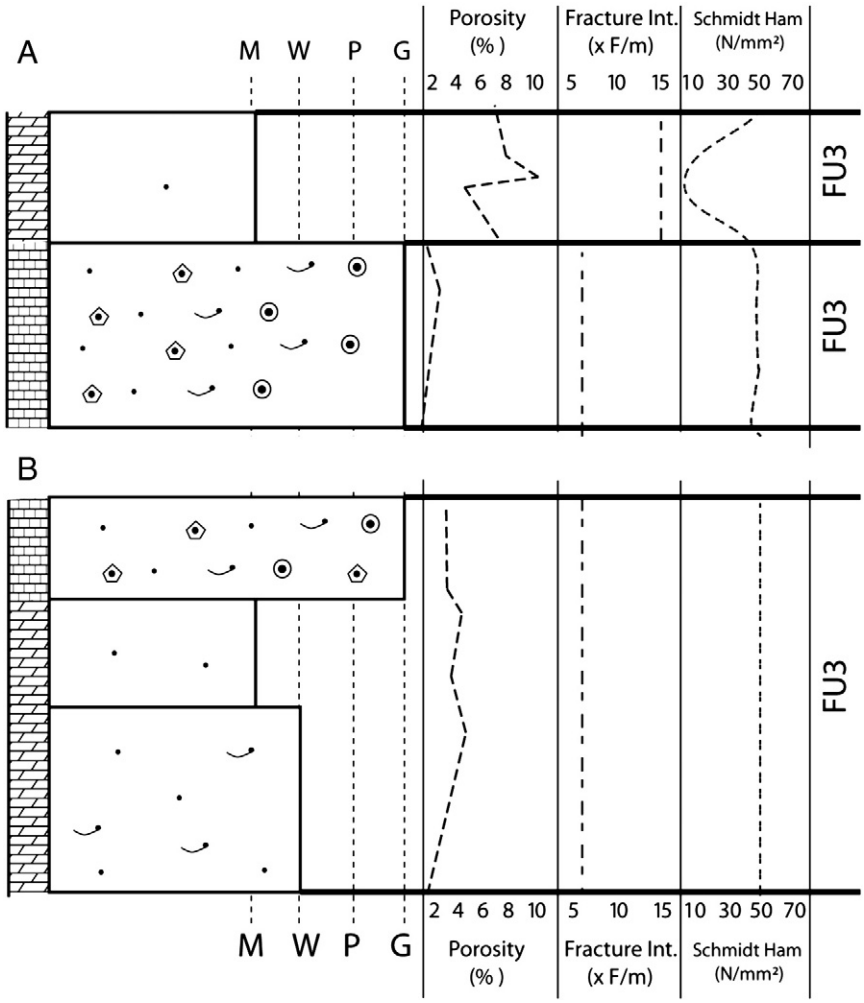

Fig. 7. Correlation of porosity evolution with the fracture intensity and mechanical properties (Schmidt Hammer rebound) across an intertidal facies sequence with contracted petrophysical properties in (A) and a subitdal facies sequence with homogeneous petrophysical properties in (B). Modified from Barbier et al. (2012a, 2012b).

of the calcite crystals (Fig. 9F). This fact allows us to further distinguish them in Type 10a (within the crystal cores) and Type 10b (at the crystal boundaries).

5.2. Fluid inclusions behavior during microthermometry

Monophase aqueous FIs (Types 1 to 5, 7, 9) were treated by quick cooling runs and by long-lasting heating runs to induce thermal re-equilibration and leakage. The few biphase FI obtained in that way were used to investigate fluid salinity.

Upon cooling after homogenization in most of Type 10 FIs, a gas phase nucleated between 35 and 60 °C, but one third of these FIs showed metastable absence of the bubble at room temperature. This explains their coexistence with monophase Type 9 FIs in the crystal cores. Cooling runs on Type 10 FIs induced ice formation during the first cooling run at temperatures between −31.5 °C and −39.8 °C. Slow reheating of Type 10 FIs could not reveal any apparent eutectic or peritectic melting. The final melting of ice was observed in both stable and metastable conditions (Table 1), the latter furnishing lower constraints to the real fluid salinity. The same melting behavior was observed in leaked biphase aqueous FIs (Types 1 to 5, 7, 9) used to determine salinity only.

Homogenization of hydrocarbon FIs (Type 6, 8) occurred in the liquid phase. Upon cooling after homogenization the gas phase nucleated in a narrow range of temperatures for both FI types, i.e. between and 15 °C and 5 °C. Cooling runs conducted on tri-phase hydrocarbon FIs (some Type 8) indicated ice nucleation by gas bubble contraction in a consistent range of temperatures (−38.6 to −39 °C) therefore similar to Type 10 FIs.

5.3. Results of microthermometry

Table 1 summarizes the main results of the microthermometric analysis. Histograms of homogenization temperatures for biphase FIs are shown in Fig. 10.

5.3.1. Fluid inclusions in host rock cements

The monophase all-liquid nature of Types 1 to 4 FIs from early dolomites, syntaxial and sparry calcites crystals indicates low temperature (<50–55 °C) of trapping (Goldstein and Reynolds, 1994). The few measurements of Tm_i on leaked bi-phase Type 1 FIs (Table 1), indicate salinity values around 240 wt.‰ NaCl equivalent suggesting hypersaline conditions of precipitation. However, some salinity values are in the range of gypsum precipitation, not the calcite precipitation (Warren, 2006), suggesting an erroneous value. Type 2 and 3 FIs, located respectively in the dolomite cores and dolomite external rims, have mode salinity values at 240 and 40 wt.‰ NaCl equivalent respectively (Table 1). The range and mode values of the Tm_i and the Tm_{imet} for both FI types overlap each other. Finally, Type 4 FIs in

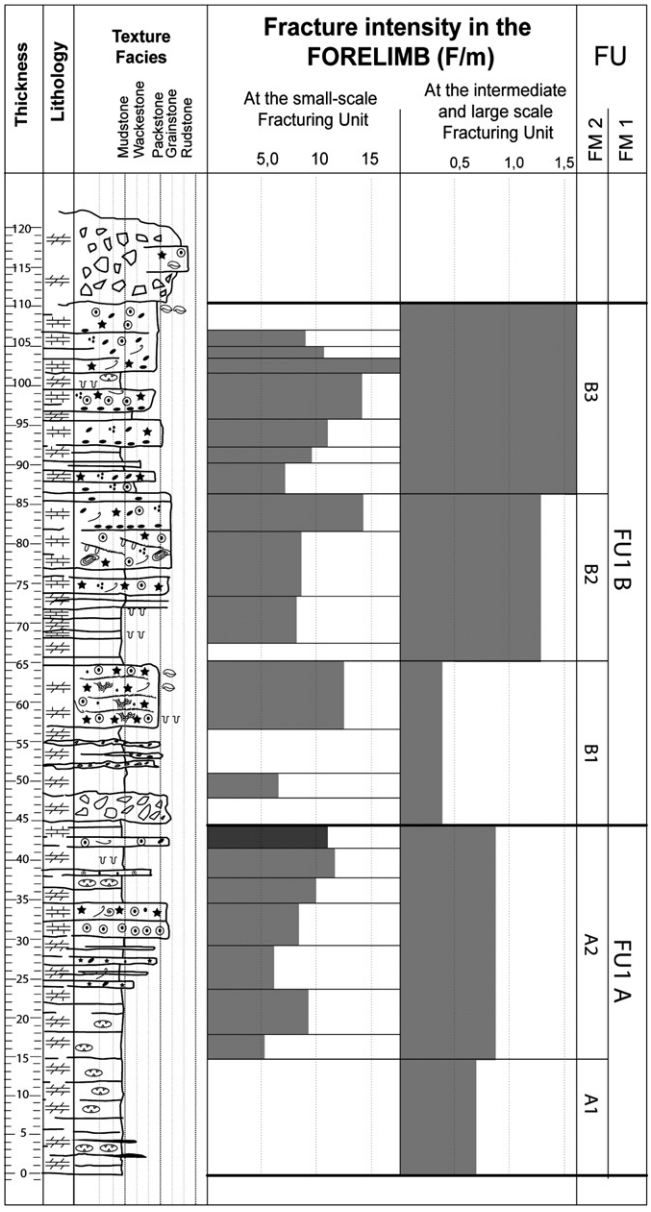

Fig. 8. Fracture stratigraphy of the lower part of the Madison Limestone for the forelimb of the Rattlesnake Mountain Anticline. The mean fracture intensity has been measured for each small-scale and intermediate fracturing units. Note the decrease in FU2 number compared to Sheep Mountain.

the sparry calcite displays a large spread in the salinity values with two modes at 15 and 80 wt.‰ NaCl equivalents.

5.3.2. Fluid inclusions in Sets I and II veins

Type 5 and Type 7 FIs in calcites of Sets I and II exhibit several features. They both suggest low trapping temperatures, although vapor phase metastability at room temperature cannot be excluded. With a few exceptions only they trapped fluids with similar low salinities (5 wt.‰ NaCl equivalent). The positive Tm_{met} of Type V FIs also suggests very low saline fluids.

Secondary Type 6 FIs record an oil migration event at temperatures above 50 °C, which are in line with those reported by primary Type 8 FIs in the calcite of Set III (Table 1). These two different types of FIs have common green fluorescence (30–40API) and similar behavior during cooling after homogenization, and support the hypothesis of a unique oil charging episode, recorded in primary Type 8 and in secondary Type 6 FIs.

5.3.3. Fluid inclusions in Set III veins

The calcite of Set III veins records a more complex fluid evolution. Monophase aqueous and poorly saline Type 9 FIs coexist (in crystal cores) with Type 8 bi-phase green fluorescing oil FIs (30–40 API), mainly homogenizing between 40 and 70 °C (mode is 55–60 °C). The aqueous fraction of the less common tri-phase green fluorescing FIs display similar salinities of 5 wt.‰ NaCl equivalent (Table 1). Also bi-phase aqueous Type 10a FIs occur in crystal cores, with Th mode around 75 °C and salinities of 5 wt.‰ NaCl equivalent (Table 1).

The metastability of gas nucleation recorded in the Type 10a FIs allows us to consider them as derived from the same low-salinity and moderately warm fluid as Type 9 FIs, i.e. the monophase FIs would correspond to the bi-phase FIs lacking a vapor bubble at room temperature because of metastability.

The similarity in salinity and the petrographic distribution within crystal cores allow associating also the hydrocarbon FIs to the same fluid event. According to this scenario an aqueous dominated fluid, locally carrying oil, was recorded by Types 8 to 10a FIs, which were trapped at the same time, i.e. during the formation of Set III veins. In this respect the Th of Type 8 oil FIs can be considered as minimum trapping temperatures.

The bi-phase aqueous FIs of Type 10b are mostly observed at the borders of the same calcite crystals filling the Set III veins. They record higher homogenization temperatures (Th mode is 120 °C) and low salinities (5 wt.‰ NaCl equivalent), and possibly represent the result of crystal border recrystallization and FI refill. There is a good correlation between the higher temperatures recorded in aqueous Type 10b FIs of Set III veins and those reported by Katz et al. (2006) and Beaudoin et al. (2011). They measured similar Th in calcite phases related to the fold amplification and exhumation phase, i.e. hydrothermal breccias and Set III fractures, respectively. No Tm_i comparison was possible because both authors refer to metastable FI behavior, which could only suggest low fluid salinities (<5 wt.‰ NaCl equivalent).

6. Diagenetic evolution

The paragenetic sequence reconstructed by Barbier et al. (2012b) was complemented by isotopic analyses to properly trace the parent fluid of the carbonate phases, and the paleofluid system evolution through space and time.

6.1. Oxygen and carbon stable isotopes

Following the results of Barbier et al. (2012b) and Barbier (2012), in both fold, the brachiopod shell calcite and the syntaxial calcite cement present an isotopic composition ($-5‰ < \delta^{18}O_{PDB} < -2‰$, $+2‰ < \delta^{13}C_{PDB} < +6‰$; Fig. 11) characteristic of marine Mississippian calcites (Veizer et al., 1999). Eogenesis in muddy supratidal facies is characterized by an extensive dolomitization whose dolomite crystals exhibit stable isotope values ranging from −3‰ to +4‰ in $\delta^{18}O_{PDB}$ and from +2‰ to +4‰ in $\delta^{13}C_{PDB}$ (Fig. 11). These positive $\delta^{18}O_{PDB}$ values reflect an isotopic fractionation due to evaporitic processes, typical of supratidal environments. The fluid inclusion melting temperature of Type 2 FIs in the dolomite cores emphasized the initial very high salinities associated to this mechanism, whereas Type 3 FIs are considered to represent the percolation of marine waters during the Osagean Transgression. Stable isotopes of the sparry calcite cements are shifted compared to the marine Mississippian calcite values. These cements, post-dating the Mississippian karstification episodes and the mechanical compaction (Barbier, 2012), exhibit a decrease from −5.79‰ to −11.73‰ in $\delta^{18}O_{PDB}$ and from +2.53‰ to +0.98‰ in $\delta^{13}C_{PDB}$ (Fig. 11). According to Goldstein and Reynolds (1994) homogenization temperatures of monophase fluid inclusions are lower than 55 °C. In a fractionation diagrams, sparry

Table 1
Petrographic features of the main types of fluid inclusions (FIs). The inclusion size is given as length in μm. F stands for the volume fraction of the liquid phase at room temperature relative to the FI total volume. L, G and O stand for aqueous liquid, gas and oil, respectively. The petrographic distribution of individual fluid inclusion assemblages (FIA) is indicated as follows: N = no particular distribution, I = isolated, C = shape and distribution controlled by crystallographic planes, R = located in clear inclusion-poor zonation rims, Dc = located in dark inclusion-rich crystal cores, Ps = along pseudo-secondary trails, V = controlled by the opening of the veins, P = in patchy concentrations, S = secondary trails. Main results of microthermometry, i.e., range and mode values of homogenization temperatures (Th), ice melting temperatures in stable (Tm_i) and metastable (Tmmet) conditions. In brackets is the number of measurements accomplished for each of the three parameters. Salinity was calculated from stable melting temperatures only and is expressed in wt.% NaCl eq. (Bodnar, 1983).

Sample	Mineral phase	FI-type	Fluid phases	FIA	Size	F	Th (°C)		Tm_i (°C)		Tm_{met} (°C)		Salinity	
							Mode	Range	Mode	Range	Mode	Range	Mode	Range
SM6.16	Syntax.	*I*	L	I/P/PS	5–7	1	–	–	−23 (5)	−21/−23	–	–	24	23.0/24.3
	Cal II	*VII*	L	C/N	2–5	1	–	–	−0.2 (5)	−0.2/−1.2	−0.2 (3)	0/−0.2	0.4	0.4/1.2
SM6.18	Dol-core	*II*	L	Dc/C/I	3–6	1	–	–	−23 (6)	−11/−40	−21 (12)	−11/−35	24	15.0/36.1
	Dol−rim	*III*	L	R/C/I	2–3	1	–	–	−2.5 (6)	−2.1/−5.5	-2.5(5)	−2/−5	4	3.5/8.5
	Cal II	*VII*	L	P/I/C	5–6	1	–	–	−0.3 (7)	−0.2/−5.5	(2)	−0.2/−2	0.5	0.4/8.5
SM4.38	Sparry	*IV*	L	N/P	3–10	1	–	–	−5 (18)	−0.4/−8	−0.3 (3)	−0.7/0	8	0.7/25
	Cal I	*V*	L	P/I/C	3–11	1	–	–	−0.2 (4)	−0.2/−0.4	–	>0	0.4	0.4/0.7
		VI	O+G(+L)	S	3–20	0.64/0.81	50 (31)	32/67	–	–	–	–	–	–
	Cal III	*VIII*	O+G(+L)	C/V/I	2–5	0.64/0.81	55 (14)	51/57	–	–	–	–	–	–
SM2.08	Cal III	*VIII*	O+G+L	N/C	4–23	0.69/0.84	55 (13)	40/82	−0.3 (3)	−0.3/−0.4	–	–	0.5	0.5/0.7
		X(a)	L+G	P/I/C	2–8	0.62/0.75	75 (21)	65/85	−0.3 (7)	−0.2/−0.4	−0.3 (14)	−0.2/−0.4	0.5	0.2/0.7
		X(b)	L+G	P/I/C	2–8	0.72/0.81	120 (56)	105/135	−0.3 (3)	−0.2/−0.3	−0.3 (54)	−0.1/−0.3	0.5	0.2/0.5
SM5.08	Cal III	*VIII*	O+G(+L)	C/Ps/N	2–13	0.7/0.84	65 (40)	41/69	–	–	–	–	–	–
		IX	L	P	4–5	1	–	–	−0.2 (2)	−0.1/−0.2	–	–	0.4	0.2/0.4
SM5.16	Syntax.	*I*	L	P	4–5	1	–	–	−23 (3)	−22.5/−23	–	–	24	24/24.3
	Sparry	*IV*	L	N/P	4–20	1	–	–	−0.9 (4)	−0.3/−1.9	–	–	1.5	0.5/3.2

calcite cements are crystallized from meteoric fluids with $\delta^{18}O_{SMOW}$ ranging from −2 to −10‰ (Fig. 12). However, salinity values are ranging from 15 wt.‰ NaCl equivalent (meteoric fluid) to 75 wt.‰ NaCl equivalent (marine fluid) that may be due to the Madison evaporite dissolutions during the Mississippian Karst and during burial. As the Madison Formation is rapidly sealed by the Amsden Formation, the crystallization of these sparry calcite cements is considered to occur in a closed diagenetic system until the Sevier Orogeny (see below).

The blocky calcite cement occurring in the early fracture set at Sheep Mountain (Sets I and II) show isotopic data in agreement with the published results of Katz et al. (2006) and Beaudoin et al. (2011), with $\delta^{18}O_{PDB}$ values ranging from −13.96‰ to −10.84‰, and $\delta^{13}C_{PDB}$ values ranging from +1.17‰ to +2.70‰ (Fig. 11). Considering homogenization temperatures lower than 55 °C (monophase FIs) and these isotopic compositions, the blocky calcite cement crystallized in Sets I and II from meteoric fluids with $\delta^{18}O_{SMOW}$ lower than −6‰ (Fig. 12). Moreover, salinity values (4 to 21 wt.‰ NaCl equivalent with a mode at 5 wt.‰ NaCl equivalent) confirm this hypothesis. At Rattlesnake Mountain, the early fracture set (NS predating the Laramide fold-perpendicular set) are healed by a blocky calcite cement that show the most depleted composition ($-25‰ < \delta^{18}O_{PDB} < -18‰$, $-1‰ < \delta^{13}C_{PDB} < 3‰$), in agreement with Beaudoin et al. (2011).

The blocky calcite cement in syn-folding Set III veins at Sheep Mountain show isotopic composition ranging from −21.23‰ to −19.71‰ in $\delta^{18}O_{PDB}$ and from −9.56‰ to −5.21‰ in $\delta^{13}C_{PDB}$ (Fig. 11). Considering the homogenization temperatures from 70 to 120 °C, the low salinity (5 wt.‰ NaCl equivalent) and these isotopic compositions, the blocky calcite cement may be crystallized in Set III from meteoric fluids with $\delta^{18}O_{SMOW}$ ranging from −6‰ to −12‰ (Fig. 12). At Rattlesnake Mountain, the syn-folding Set III veins show less depleted compositions (from −15‰ to −13‰ in $\delta^{18}O_{PDB}$ and from −1‰ to +1,4‰ in $\delta^{13}C_{PDB}$) in regarding the early Sets I and II (Fig. 11).

In a general view, at Sheep Mountain, the isotopic composition both in $\delta^{18}O_{PDB}$ and $\delta^{13}C_{PDB}$ of the blocky calcite cements are shifted toward negative values whereas at Rattlesnake Mountain, the most negative values are obtained during Sets I and II formation and then get back to less negative isotopic compositions during syn-folding Set III formation (Fig. 11). At Rattlesnake Mountain, the isotopic compositions from the three main vein sets are in line with the burial trend and appear to be less contaminated by light carbon influx supposedly stemming from hydrocarbon migration (in agreement with the lack of oil charge evidences in the Madison Limestone in Rattlesnake Mountain).

6.2. Strontium isotopes

The $^{87}Sr/^{86}Sr$ ratios have been measured for both Set II (4 veins) and Set III (3 veins) calcites, plotted against the $\delta^{18}O_{PDB}$ compositions of these fracture cements, and compared to the existing data of Katz et al. (2006) and Beaudoin et al. (2011) (Fig. 13). We also added the marine Mississippian calcite composition (Bruckschen et al., 1999; Mii et al., 1999), as well as the estimate Paleogene meteoric calcite cements from Rhodes et al. (2002), contemporaneous with the Laramide folding. Calcites from Sets II and III show enrichment in radiogenic strontium ($0.7085 < {}^{87}Sr/^{86}Sr < 0.7092$) compared to marine Mississippian calcite (Fig. 13) in agreement with published data (Beaudoin et al., 2011; Katz et al., 2006). Moreover, these two blocky calcite cements exhibit the same $^{87}Sr/^{86}Sr$ ratios that could reflect crystallization from similar meteoric fluids but at different pressures and temperature conditions.

7. Discussion: toward a scenario of rock fluid interaction during folding

7.1. Origin of the involved fluids

7.1.1. Origin of the involved fluid of host rock cements

Salinity values of Type 2 FIs indicate hypersaline conditions that are in agreement with the fact that these FIs are observed in dolomite crystal occurring within supratidal sabkha facies (Barbier et al., 2012a, 2012b). This evaporitic environment is considered to be associated to a seepage reflux phenomenon. The contrasted low salinities of FIs located in the rims of dolosparites crystals (Type 3) are interpreted to reflect a dilution of the supersaturated evaporitic Mississippian fluid. According to the petrographic and stratigraphic analysis as well as the salinity values (40 wt.‰ NaCl equivalent), these rims are interpreted to pass during shallow burial conditions from marine fluids with normal salinities. The crystallization of these rims could have occurred during the marine transgression in the Osagean. Finally, the sparry calcite cements crystallized during burial from pore water in a closed diagenetic system until the Sevier Orogeny (Cenomanian, see above Section 6.1).

7.1.2. Origin and timing of the involved fluid of the Sets I to III blocky calcite cements

Blocky calcite cements in veins crystallized from meteoric fluids with a $\delta^{18}O_{SMOW}$ composition lower than −6‰ (see Section 5.1). According to the fractionation diagram (Fig. 12), these meteoric fluids are different from those at the origin of the host rock sparry calcite cements. Moreover, salinity values of blocky calcite cements are around 5 wt.‰ NaCl equivalent, whereas salinity values range from 5 to 75 wt.‰ NaCl equivalent for the host rock sparry calcite cements. These results suggest the percolation *per descensum* of less saline meteoric fluids through time after the crystallization of the sparry calcite cements. Strontium isotopic data of the blocky calcite cements (0.7087 to 0.7092) are less radiogenic compared to the calcite cements crystallized from the Palaeocene surface meteoric waters (0.71199 to 0.71331, Fig. 13; Rhodes et al., 2002) and therefore, suggest that blocky calcite cements did not crystallized from these fluids.

The Ouachita–Marathon Orogeny at the end of the Pennsylvanian could have contributed to the percolation of meteoric waters in the North America Marge. However, in Wyoming, this orogeny involved only the percolation down to the Pennsylvanian and Permian series that were always under marine influences (Kluth and Coney, 1981; Kluth and Peterson, 1986; Maughan, 1993). An alternative scenario

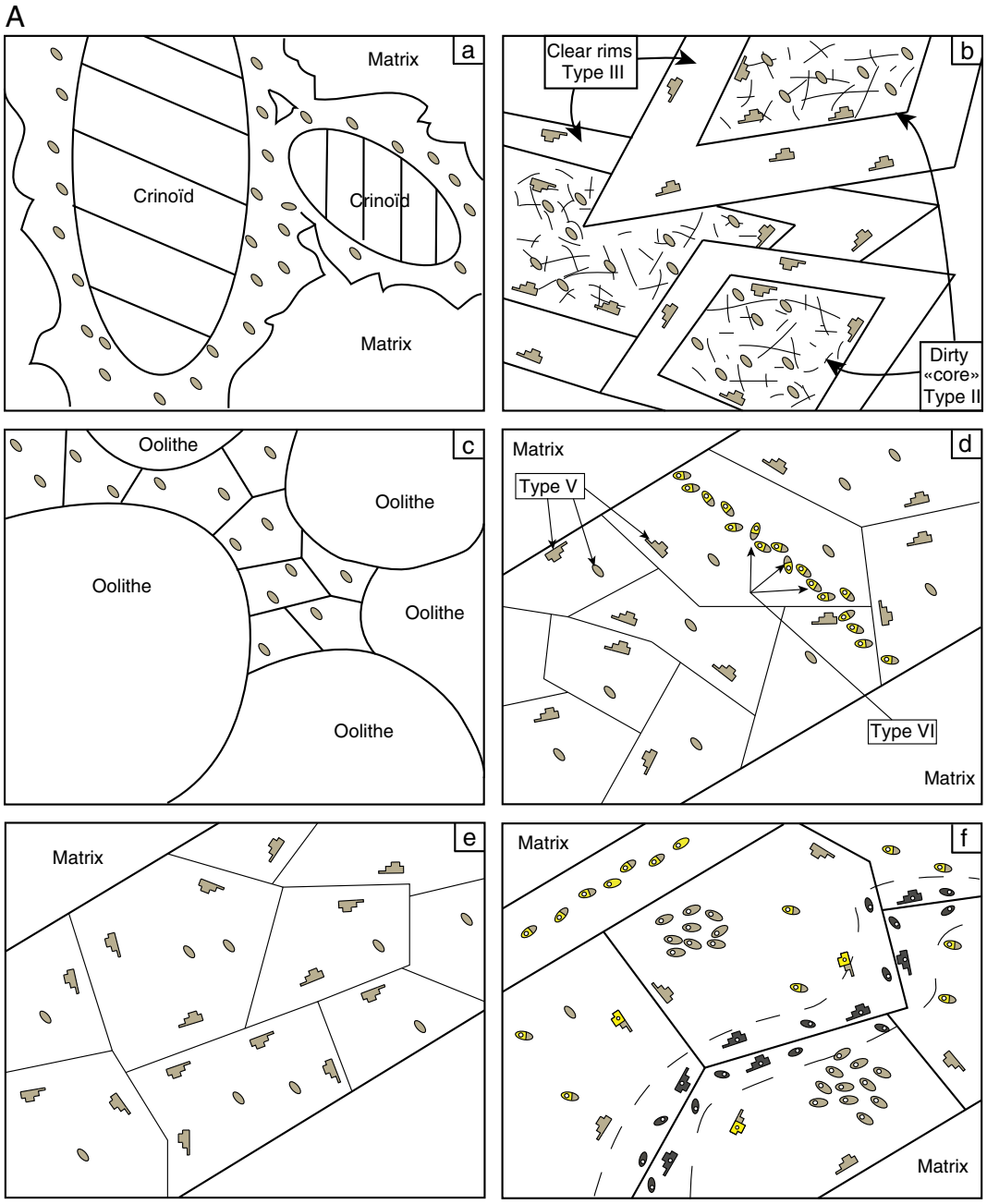

Fig. 9. A: Sketch illustrating the location and distribution of the different FI types in the various diagenetic phases. a) Type 1 in syntaxial calcites. b) Type 2 and Type 3 in dolomite cloudy cores and clear rims, respectively. c) Type 4 in sparry calcites. d) Primary aqueous Type 5 and secondary oil bearing Type 6 in Set I calcite. e) Type 7 in Set II vein calcite. f) Aqueous monophase Type 9 and biphase Type 10a within the crystal cores of Set III calcite coexist with oil bearing Type 8, locally controlled by fracture re-opening. Type 10b aqueous FIs are mainly concentrated in the calcite crystal borders. B: Pictures illustrating the fluid inclusion petrography: a) Type 1 FI in syntaxial calcite (scale bar 100 μm); b: Type 2 and 3 in dolomites cloudy cores and clear reams respectively (100 and 20 μm); c: Type 4 in sparry calcite (20 μm); d: Primary type 5 and secondary oil-bearing type 6 in set I calcite (20 μm); e: Type 7 in set II vein calcite (100 μm); f: Aqueous monophase Type 9 (100 μm) and biphase Type 10a (20 μm) within the crystal cores of Set III calcite coexist with oil bearing Type 8 (20 μm), locally controlled by fracture re-opening. Type 10b aqueous FIs (100 μm) are mainly concentrated in the calcite crystal borders.

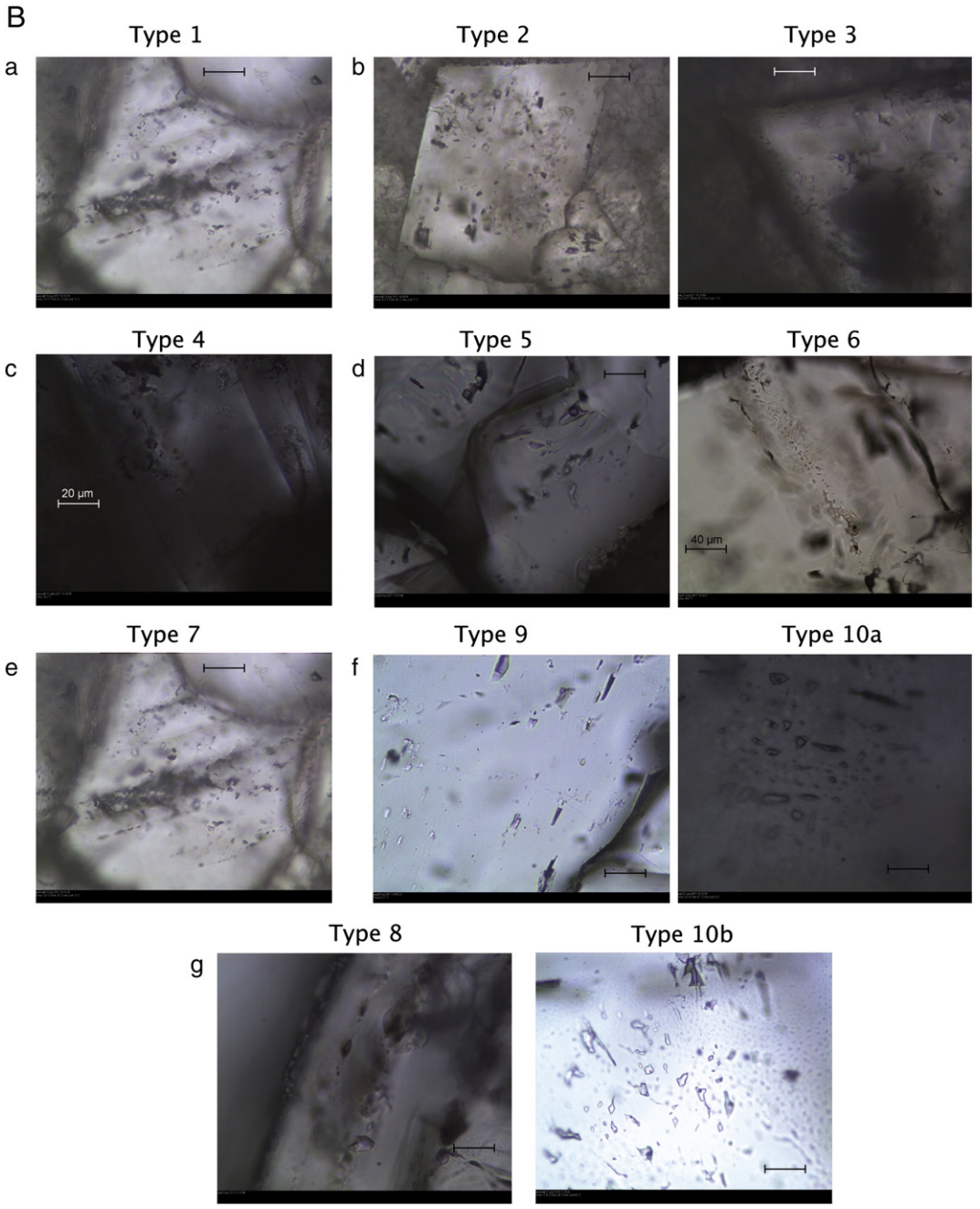

Fig. 9 (*continued*).

suggests that the Sevier Orogeny in Wyoming may have contributed to the recharge in meteoric fluids of the Madison Formation by lateral migration of fluids (~−115 to −80 Ma). With this hypothesis, the enrichment in radiogenic strontium of blocky calcite cements (0.7087 to 0.7092) compared to the marine Cenozoic calcite (0.7082 to 0.7068) (McArthur and Howarth, 2004), could reflect the percolation of Cenozoic meteoric fluids through the Jurassic to Pennsylvanian underlying series. At the beginning of the Sevier Orogeny, the Teton Range and Wind River Range were already exhumed (Royse, 1993), and thus may have been potential meteoric recharge zones. A lateral migration of meteoric fluids of more than 100 km toward the North–East to Sheep Mountain may have occurred during 20 to 30 My in maximum, from the Aptian (beginning of the Sevier Orogeny in Wyoming, Royse, 1993) to the Campanian (age of the beginning of the Laramide Orogeny, Bird, 1998). In this case, this would correspond to minimum migration rates ranging from 4 to 6 km/My. These estimations are compatible with the estimations of Schneider (2003) for both the Canada (2 km/My) and Venezuela Foothills (5 to 20 km/My).

The presence of primary oil-inclusions within blocky calcite cements of Set III and secondary oil-inclusions within blocky calcite cements of Set I indicate a hydrocarbon migration during the Laramide folding of Sheep Mountain. This hydrocarbon migration may have contaminated the meteoric fluids in $\delta^{12}C$ which could explain the very low $\delta^{13}C_{PBD}$ of blocky calcite cements within both the through-going Set III veins and the re-opened portions of Set I veins (Fig. 11).

Rattlesnake Mountain shows a quite similar pattern of fluid origin, although the highest depletion in stable isotope correspond to the early fracture set, formed as a response to the Sevier shortening phase (Beaudoin et al., 2012–this issue), and probably at a maximum burial deeper than for Sheep Mountain. But, the fact that the calcite cements of Set I veins present the most depleted data (Fig. 11), whereas the calcite cements of the syn-folding Sets II and III show higher $\delta^{18}O_{PDB}$

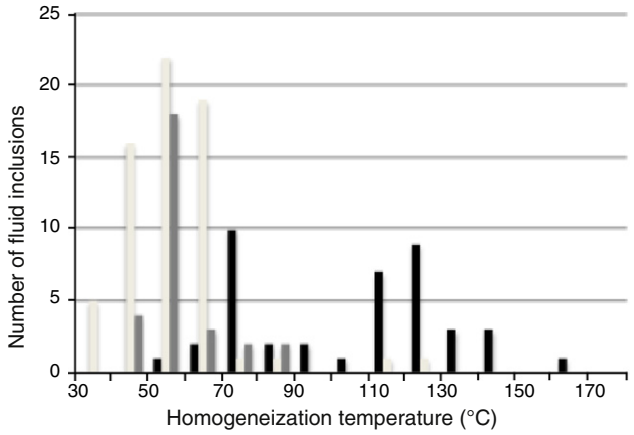

Fig. 10. A) Homogenization temperatures of aqueous bi-phase FI types from the blocky calcite cements of Set III veins (black). B) Homogenization temperatures of oil-bearing tri-phase FI types from from the blocky calcite cements of Set III veins (light gray) and set I veins (dark gray).

isotopic values, points toward an early invasion of the Set I fracture network by deep formational fluid. This invasion during the early history of basin shortening, relates to the proximity to the mountain front, which also controlled also the fracturing process. The fracture network, which is at all-times persistent and connecting the various reservoir units, allows for a large scale homogenization of the fluid.

Homogenization temperatures are modified with respect to trapping temperature by the pressure of entrapment (Fig. 14). Calculations were accomplished in order to apply a geologically coherent pressure correction to the Th mode value obtained from the different Sets of veins FIs. Mode salinity values were used for isochore calculation. According to a maximum burial of 2.2 to 3.0 km (Amrouch et al., 2011; Hennier and Spang, 1983; Neely and Erslev, 2009) in hydrostatic conditions (10 MPa/km), a maximum fluid pressure of 22–30 MPa is deduced. At such conditions, the expected temperature is ranging from 63 to 87 °C with a geothermal gradient of 29 °C/km (Brigaud et al., 1990). However, according to Amrouch et al. (2011), the fluid overpressure increased with the deformation and reached a maximum of 19 MPa during the Set II pre-folding veins formation until the Set III formation. In a P–T diagram, the intersection point between the constructed isochore and the maximum pressures furnishes the maximum upper constraint for the FIs trapping temperatures (Fig. 14). Homogenization temperature corrections for FIs Type 5, occurring within blocky calcite cements of Sets I veins, display temperatures ranging from 65 °C to 75 °C (Fig. 14). These temperatures increase until 75 to 80 °C in Type 7 FIs due to the increase of fluid overpressure (+19 MPa) during Set II vein formations. In the same way, homogenization temperature corrections of FIs Type 9 and 10a, occurring within blocky calcite cements of Set III veins, display temperatures

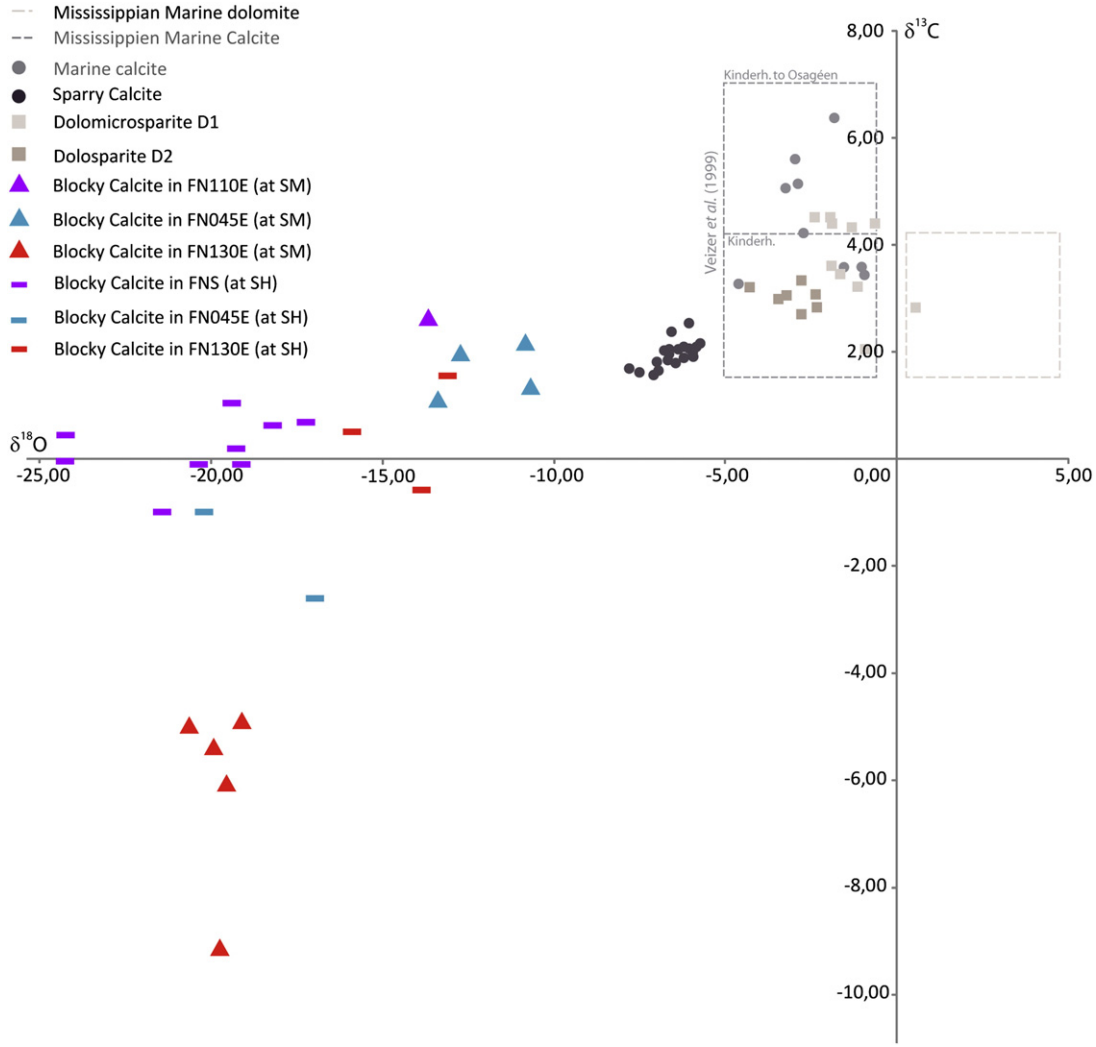

Fig. 11. Stable isotopic data for the two anticlines. Mississippian marine calcite are from Veizer et al. (1999). Note the most depleted $\delta^{18}O_{PDB}$ isotopic compositions are observed in Laramide folding fractures (Set III) at Sheep Mountain whereas in the Sevier fractures (Set I and II — FNS and FEW) at Rattlesnake Mountain.

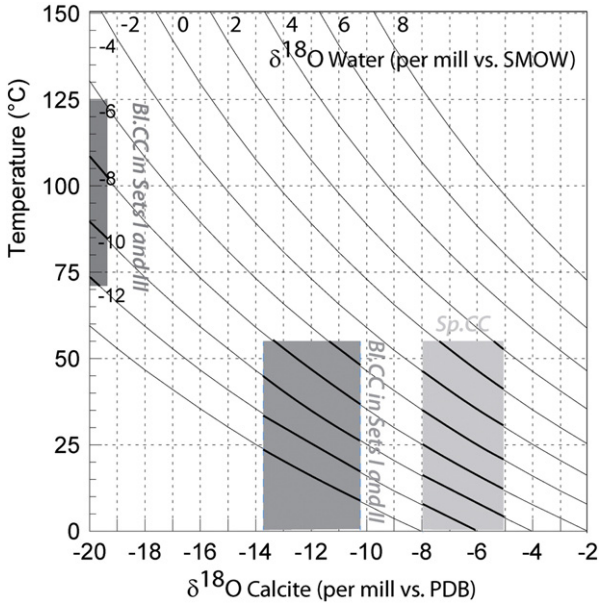

Fig. 12. Isotopic fractionation diagram from Friedman and O'Neil (1977) used to estimate the isotopic composition in $\delta^{18}O_{SMOW}$ of fluids in equilibrium with the sparry calcite cements of the host rock and the blocky calcite cements of Set II and III veins of Sheep Mountain.

ranging from 83 °C to 86 °C (Fig. 14) at 22 MPa (2200 m) and 30 MPa (3000 m) of burial. At such pressure conditions, these temperatures would indicate a local remobilization of meteoric pore fluids considering a geothermal gradient of 29 °C/km (Brigaud et al., 1990).

On the contrary, homogenization temperature corrections of FIs Type 10b, observed within blocky calcite cements of Set III veins, display temperatures of 140 °C at 30 MPa (3000 m) of burial, with a geothermal gradient ranging from 40 to 45 °C/km. These gradients are however, higher than those estimated by Brigaud et al. (1990). Indeed, these authors considered a geothermal gradient of 29 °C/km with which homogenization temperature corrections of FIs Type Xb would display temperatures ranging from 145 °C to 150 °C at 45 MPa (4500 m) to 50 MPa (5000 m) (Fig. 14). Such temperatures have been measured 20 km westward from Sheep Mountain under 4500 m of burial (Heasler and Hinckley, 1985). As Set III veins are formed during the exhumation of the Madison Limestone and folding, we can consider FIs Type Xb population to reflect the injection of hot basinal fluids, that is hydrothermal fluids *sensu* Machel and Lonnee (2002) into Sets III and re-opened Set I veins.

7.2. Fluid system evolutions in relation to contractional deformation

7.2.1. From the basin scale …

From the Antler Orogeny in Mississippian to the Sevier Orogeny in Cretaceous, the Madison Limestone was covered by 2200 m to 3000 m of impermeable silicoclastic series. The remobilization of pore fluids from the karstic episode, at the end of the Mississippian, involved porosity destruction of Mississippian carbonates by the crystallization of the sparry calcite cements (Barbier, 2012; Barbier et al., 2012b). During the Cenomanian, the compressive stress of the Sevier Orogeny formed the Teton Range and Wind River Range that probably acted as the main meteoric recharge zones in the North-West Wyoming (Fig. 15A). The formation of these reliefs during the Sevier Orogeny could be the main control to the lateral migration of the meteoric fluids toward the North–East with a minimum migration rates estimated around 4 to 6 km/My (Fig. 15A). The Madison Limestone, overlain by the impermeable Amsden Formation, was probably an excellent drain, particularly the evaporites solution breccias and dolomitic intervals respectively (Barbier, 2012; Sonnenfeld, 1996a) (Fig. 15A).

The continuum between the Sevier and Laramide Orogenies is characterized by an increase in pore fluid overpressure (+19 Mpa) at Sheep Mountain in Set II veins (Amrouch et al., 2011). The increase of the compressive stress, the low persistence of neo-formed veins (Set II), and the fact that the Madison Limestone is rapidly sealed by the Amsden Formation are favorable conditions to the increase of pore fluid pressure. Indeed, the stratabound character of Sets II at the maximum burial probably limited the vertical migration of fluids, allowing an increase in pore fluid pressure at the beginning of the Laramide Orogeny. The Bighorn Basin formed with the increase in the compressive stress of the Laramide Orogeny during the Paleocene, and subsequently the Madison Limestone was buried at

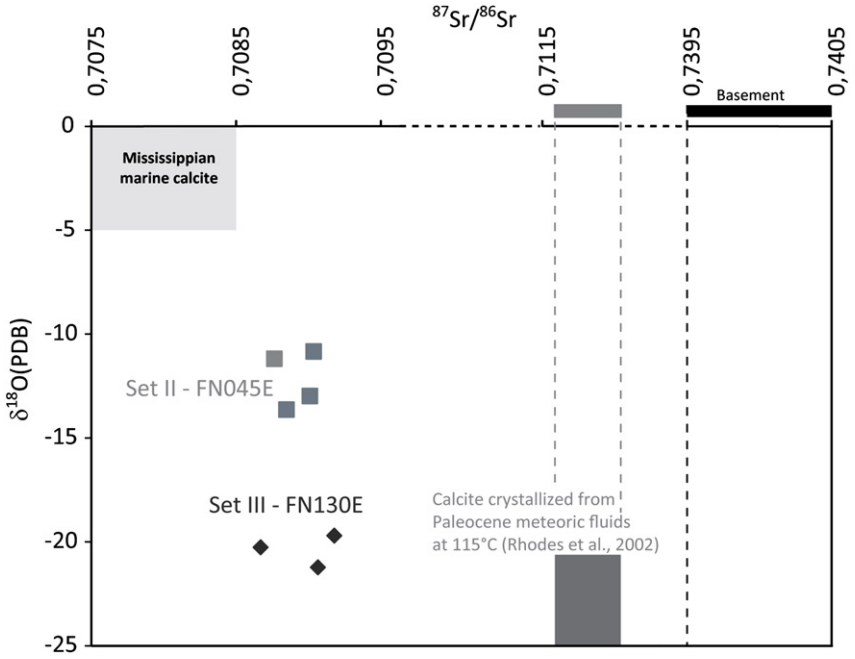

Fig. 13. $^{87}Sr/^{86}Sr$ isotopic ratio versus stable isotopic $\delta^{18}O_{PDB}$ values for the blocky calcite cements of Set II and III veins of Sheep Mountain. Marine Mississippian calcite values are from McArthur and Howarth (2004). The Paleocene meteoric calcite data and Precambrian basement values are reported from Rhodes et al. (2002).

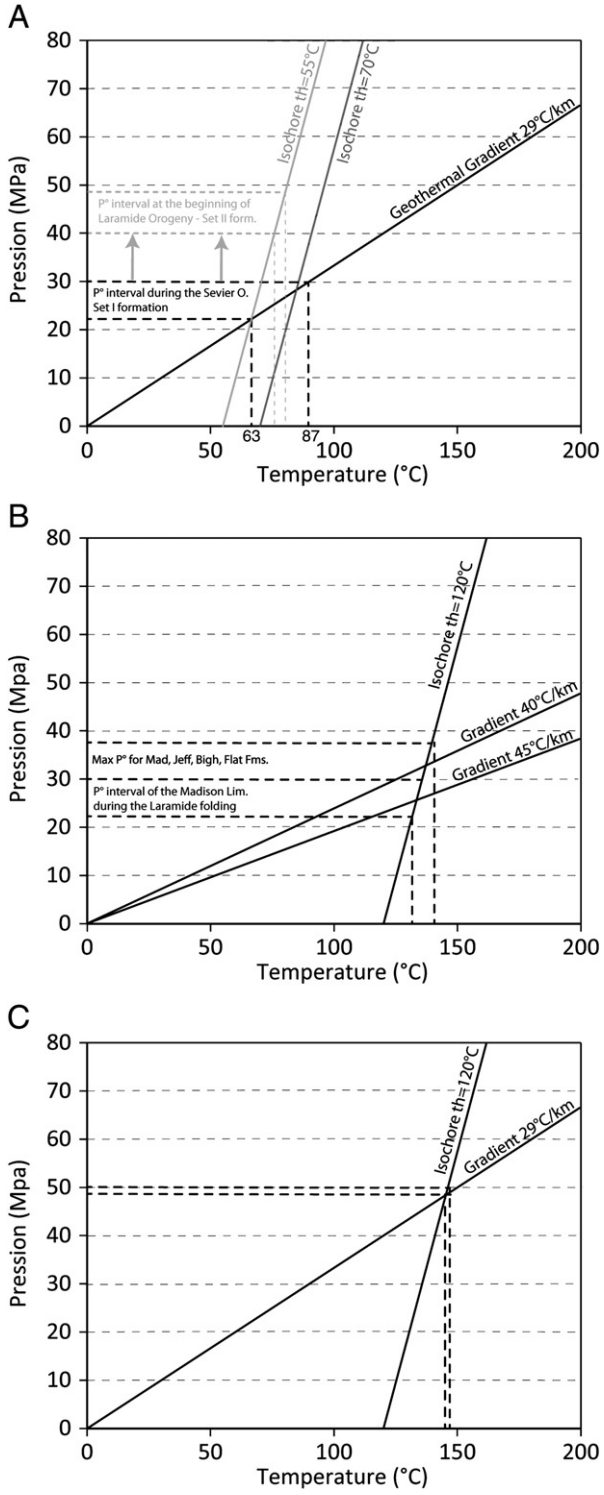

Fig. 14. Homogenization temperature corrections of fluid inclusions Type 5 to 10b as a function of the pressure and temperature. A) Homogenization temperature corrections for FIs Types 5 to 9. B) Homogenization temperature corrections for FIs Type 10b with an abnormal geothermal gradient of 40 °C/km at 30 MPa. C) Homogenization temperature corrections for FIs Type 10b with a normal geothermal gradient of 29 °C/km at 45–50 MPa.

6000 m in its center and only under 1000 m of series along its flanks (Heasler and Hinckley, 1985) (Fig. 15B). As a consequence, lithostatic pressure differences and compressive laramide stress may have been the main driving forces for hot oil-charged fluids migration from the basin to the surface such as at Sheep Mountain (Fig. 15A, B). These hot fluids may have migrated laterally along evaporites solution breccias and dolomitic intervals of the Madison Limestone as well as through the Ordovician and Devonian Bighorn and Three/Fork Jefferson Formations respectively (Barbier, 2012). However, these fluids did probably not migrate along basement fault systems as attested by the low strontium isotopic ratio of the blocky calcite cements (Fig. 13).

Heasler and Hinckley (1985) showed that the three resurgence zones of hydrothermal waters still existed in Wyoming: Shoshone Canyon, Wind River Canyon and Sheep Mountain. According to these authors, these meteoric fluids would stem from the basin, where they are heated, then migrate through the Paleozoic Aquifers, and finally emerge at these three locations with abnormal temperatures.

7.2.2. … to the reservoir scale

The fluid system evolution at the reservoir scale evolution at Rattlesnake Mountain and Sheep Mountain can be divided into four steps.

The first step corresponds to the progressive burial of the Madison Limestone from the time of deposition until the foreland basin maximum burial stage (roughly 2200 to 3000 m for Sheep Mountain, and 3500 m for Rattlesnake Mountain depending on the authors, *e.g.* Amrouch et al., 2010; DeCelles, 1994; Heasler and Hinckley, 1985). In the case of Sheep Mountain, the stratigraphic column exhibits highly contrasted mechanical properties, due to the early and burial diagenetic processes, and favors the confinement at various scales of fracture development (Barbier et al., 2012a, 2012b).

During the second step, in the foreland basin of the Sevier Orogeny, Set I veins formed, at the maximum burial which is estimated at 2200 to 3000 m for Sheep Mountain and up to 3500 m for Rattlesnake Mountain from the known sedimentary column (Hennier and Spang, 1983; Neely and Erslev, 2009). At Sheep Mountain, this fracture set is mainly stratabound, precluding any large scale vertical connection between the Madison Limestone and the adjacent Devonian and Pennsylvanian Formations. At that time, these fractures collected local pore fluid at temperatures ranging 66 °C to 75 °C. In the case of Rattlesnake Mountain, the Set I veins are highly persistent and connect most of the sedimentary column to the deep aquifer. Meanwhile the Chugwater Formation prevented the arrival of surface meteoric fluids. The Set I veins here present calcite cements with the most depleted $\delta^{18}O_{PDB}$ isotopic values of the entire data set, far below the Sheep Mountain ones, indicating higher temperature and suggesting an earlier mobilization of deeper fluids than at Sheep Mountain (Katz et al., 2006).

The third step corresponds to the Eocene early prefolding Set II veins (following the maximum burial) in the foreland basin of the Laramide Orogeny. Set II veins formed in relation to the Laramide compression. At Sheep Mountain, these joints are small and mostly bed-confined, whereas they are through-going at Rattlesnake Mountain. At Sheep Mountain, the isotopic values of the cements in these joints are similar to the earlier Set I cements, close to the maximum burial values and suggest again a local remobilization of the pore fluids. On the contrary, at Rattlesnake Mountain, they present values lower than the Set I joint ones but also lower than their Sheep Mountain counterparts. This suggests the beginning of exhumation but still the mobilization of deep fluids through the larger scale fractures of Set II.

During the folding fourth step, the two anticlines are exhumed and transected by the syn-folding Set III joints, which are the first ones enabling a vertical connection of deep and surficial reservoirs at Sheep Mountain (Fig. 16). At this stage, Set I joints are partly remobilized in transtension (Barbier et al., 2012a, 2012b; Bellahsen et al., 2006a), associated to the deposition of a new rim of cement similar to the Set III vein cements. Homogenization temperatures at crystal rims (Th = 120 °C) suggest hydrothermal fluids (*sensu* Machel and Lonnee, 2002) far above the expected maximum burial temperature, already lowered by folding and erosion. They present accordingly blocky calcite cements with the most depleted $\delta^{18}O_{PDB}$ isotopic values close to the most depleted $\delta^{18}O_{PDB}$ isotopic values observed for the blocky calcite cements at Rattlesnake Mountain. This

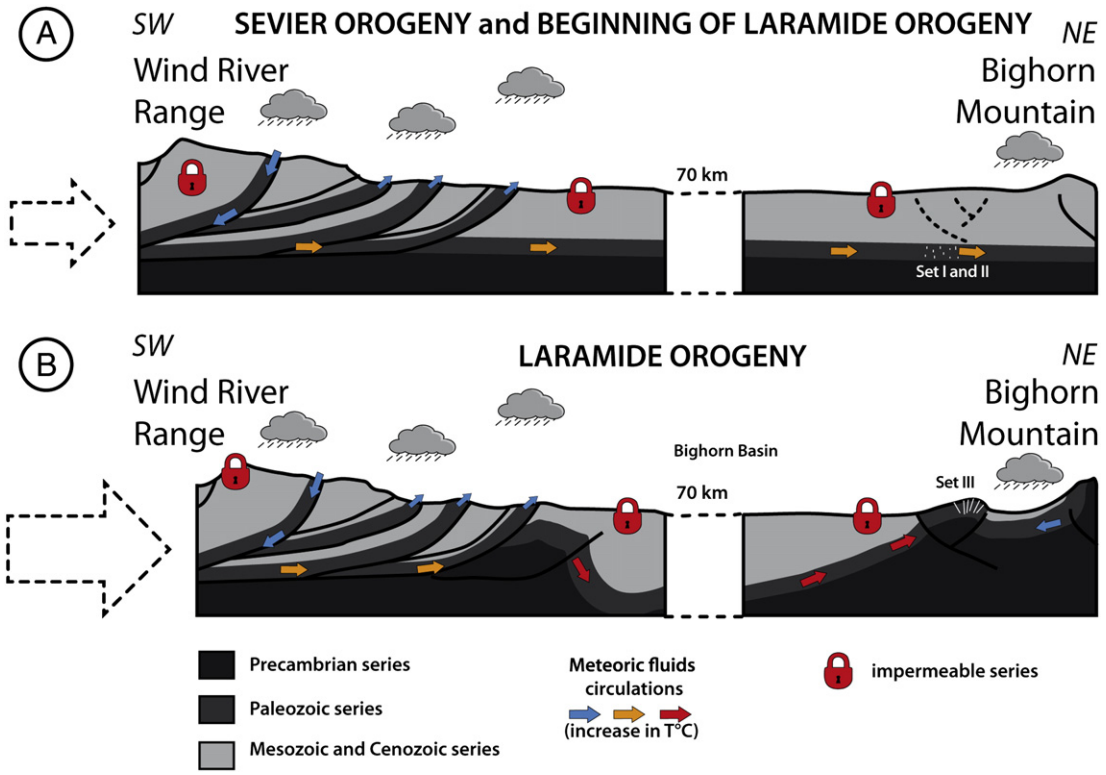

Fig. 15. Geological cross-section from the Wind River Range to the Bighorn Mountain. A) Deformation and fluid circulations related to the Sevier Orogeny during the Cenomanian. The Bighorn Basin was not already formed excepted the Wind River Range and Teton Range which could have been potential recharge zones for meteoric waters. B) Deformation and fluid circulation related to the Laramide Orogeny and Bighorn foreland basin formation during the Paleocene. The differences in lithostatic pressure and the compressive stress of the Laramide Orogeny are the main driving forces for the rapid lateral migration of hot meteoric fluids from the basin to the surface such as at Sheep Mountain Anticline.

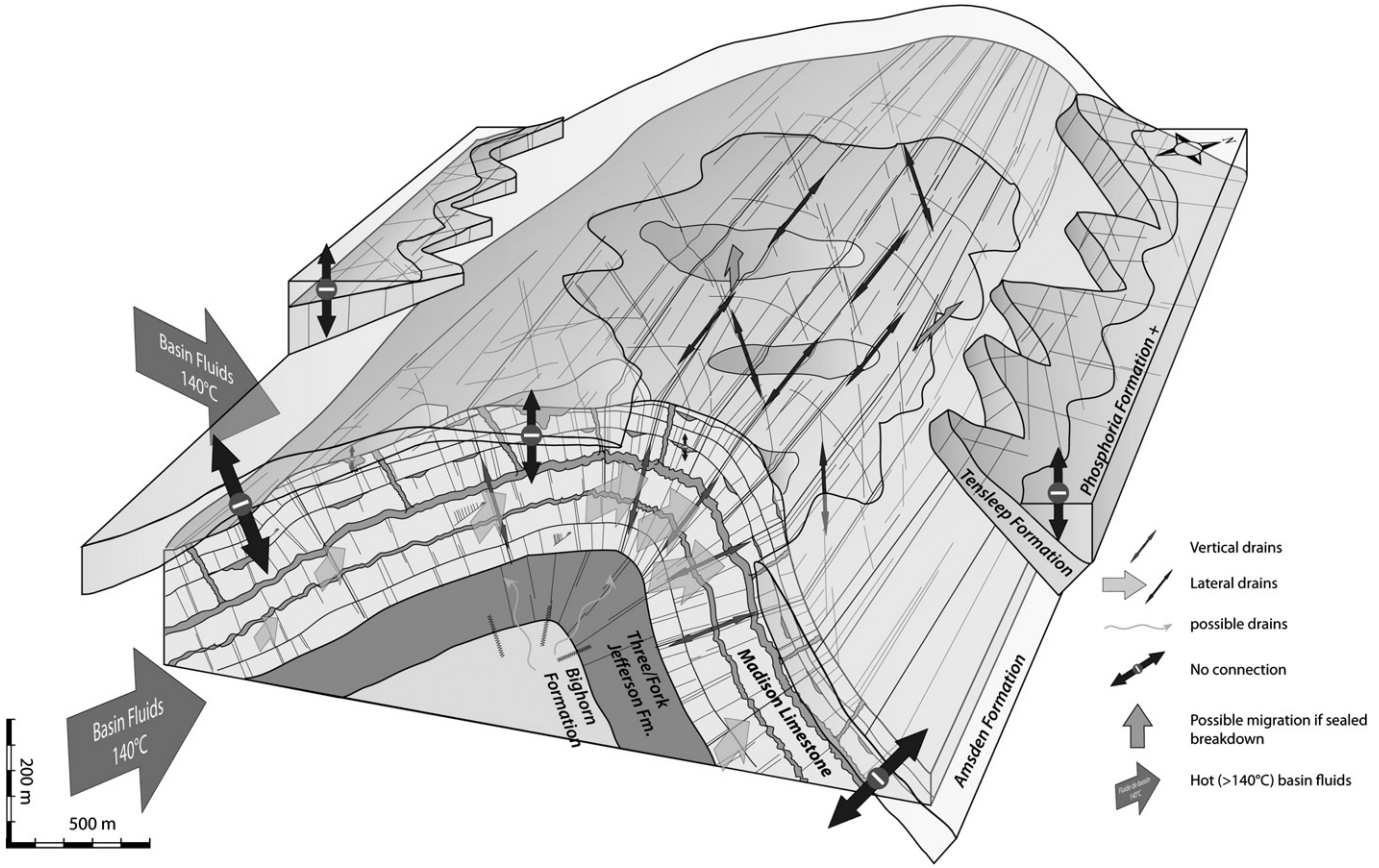

Fig. 16. Conceptual circulation fluids scenario at Sheep Mountain during folding. The formation of Set III fractures allowed efficient vertical and lateral drainage of hot basin fluids. The hinge and the forelimb are efficient fluid pathways zones.

reflects the opening of the diagenetic system, and the lateral recharge of the aquifer from pressurized deeper part of the basin (*e.g.* a squeegee fluid flow event, Beaudoin et al., 2011; Machel and Cavell, 1999). These cements also show the strongest contamination by low isotopic values in $\delta^{13}C_{PDB}$ related to oil migration and trapping. A different scenario is observed at Rattlesnake Mountain, where $\delta^{18}O_{PDB}$ isotopic values of the Set III appear less negative than the ones of the former joint sets, tied to the exhumation trend and to the progressive decrease in temperature.

8. Conclusions

In these two anticlines, the vertical connectivity between limestone formations and aquifers is achieved by the through-going vein sets that allow for the introduction of exotic meteoric fluids within the limestones, marked by contrasted isotopic composition.

This vertical connectivity can be acquired at various stages of folding, depending on the initial sedimentary succession, and its later diagenetic and structural evolution. In the case of Sheep Mountain, this occurs only during the folding episode, through the bending-related Set III veins. Here, most of the cements in the matrix and in the early vein Sets I and II, are precipitated from a fluid at temperature in equilibrium with the host rock from burial to the beginning of exhumation. The Set III veins then record the arrival of deeper and warmer meteoric fluid. By contrast, the fracture network at Rattlesnake Mountain is mostly composed of persistent veins due to a very homogeneous sedimentary-diagenetic succession. Here the vertical connectivity of the deep reservoirs and the Madison Limestone is achieved early in the history of fracturing, and the early Set I veins present very negative $\delta^{18}O_{PDB}$ cements crystallized from deepest fluids, at the time of maximum burial.

The facts presented above allow defining the fluid system evolution in relation to folding. The consistency of the gathered dataset demonstrates that fracture stratigraphy has a large impact on the hydrodynamic regime before and during folding. In particular, comparison of the evolution of Sheep Mountain and Rattlesnake Mountain anticlines shows different evolution of fluid pathways, largely controlled by the hierarchical development of fracture networks in different parts of the stratigraphic section.

Acknowledgments

We thank Pr. Michael Joachimsky at the University of Erlangen for the isotopic analysis, and Herman Ravalojaona for the high quality thin sections. We gratefully acknowledge Dr Andrea Billi and Pr. Mark P. Fischer for their helpful suggestions and remarks.

References

Ahmadahdi, F., Daniel, J.M., Azzizadeh, M., Lacombe, O., 2008. Evidence for pre-folding vein development in the Oligo-Miocene Asmari Formation in the Central Zagros Fold Belt, Iran. Tectonics 27, TC1016, http://dx.doi.org/10.1029/2006TC001978.

Amrouch, K., Lacombe, O., Bellahsen, N., Daniel, J.M., Callot, J.P., 2010. Stress/strain patterns, kinematics and deformation mechanisms in a basement-cored anticline: Sheep Mountain anticline (Wyoming, USA). Tectonics 29, TC1005, http://dx.doi.org/10.1029/2009TC002525.

Amrouch, K., Beaudoin, N., Lacombe, O., Bellahsen, N., Daniel, J.M., 2011. Paleostress magnitudes in folded sedimentary rocks. Geophysical Research Letters 38, L17301, http://dx.doi.org/10.1029/2011GL048649.

Angerer, E., Lanfranchi, P., Rogers, S.F., 2003. Fractured reservoir modeling from seismic to simulator: a reality? The Leading Edge 22, 684–689.

Bakker, R.J., 2003. Package FLUIDS 1. Computer programs for analysis of fluid inclusion data and for modelling bulk fluid properties. Chemical Geology 194, 3–23.

Bakker, R.J., 2009. Package FLUIDS. Part 3: correlations between equation of state, thermodynamics and fluid inclusions. Geofluids 9, 3–23.

Barbier, M., 2012. Hétérogénéités multi-échelles sédimentaires, diagénétiques et structurales de la Formation carbonatée Madison (Wyoming, USA), Ph.D Dissertation, Aix-Marseille University.

Barbier, M., Hamon, Y., Callot, J.P., Floquet, M., Daniel, J.M., 2012a. Sedimentary and diagenetic controls on the multiscale fracturing pattern of a carbonate reservoir: The Madison Formation (Sheep Mountain, Wyoming, USA). Marine and Petroleum Geology 29, 50–67, http://dx.doi.org/10.1016/j.marpetgeo.2011.08.009.

Barbier, M., Hamon, Y., Doligez, B., Callot, J.P., Floquet, M., Daniel, J.M., 2012b. Stochastic joint simulation of facies and diagenesis: a case study on early diagenesis of the Madison formation (Wyoming, USA). Oil and Gas Science and Technology 67 (1), 123–145, http://dx.doi.org/10.2516/ogst/2011009.

Beaudoin, N., Bellahsen, N., Lacombe, O., Emmanuel, L., 2011. Fracture-controlled paleohydrogeology in a basement-cored, fault-related fold: Sheep Mountain Anticline, Wyoming, United States. Geochemistry, Geophysics, Geosystems 12, Q06011, http://dx.doi.org/10.1029/2010GC003494.

Beaudoin, N., Leprètre, R., Bellahsen, N., Lacombe, O., Amrouch, K., Callot, J.P., Emmanuel, L., Daniel, J.M., 2012. Structural and microstructural evolution of the Rattlesnake Mountain Anticline (Wyoming, USA): new insights into the Sevier and Laramide orogenic stress build-ups in the Bighorn Basin. Tectonophysics 576–577, 20–45 (this issue).

Bellahsen, N., Fiore, P., Pollard, D.D., 2006a. The role of fracture in the structural interpretation of Sheep Mountain Anticline, Wyoming. Journal of Structural Geology 28, 850–867.

Bellahsen, N., Fiore, P.E., Pollard, D.D., 2006b. From spatial variation of fracture patterns to fold kinematics: a geomechanical approach. Geophysical Research Letters 33, 1–4.

Bergbauer, S., Pollard, D.D., 2004. A new conceptual fold-fracture model including prefolding veins, based on field data from the Emigrant Gap anticline, Wyoming. Geological Society of America Bulletin 116, 294–307.

Bird, P., 1998. Kinematic history of the Laramide Orogeny in latitudes 35 degrees–49 degrees N, western United States. Tectonics 17 (5), 780–801.

Bodnar, R.J., 1983. A method of calculating fluid inclusion volumes based on vapor bubble diameter and P-V-T-X properties of fluid inclusions. Economic Geology 78 (3), 535–542.

Bodnar, R.J., 1993. Revised equation and table for determining the freezing point depression of H2O–NaCl solutions. Geochimical et Cosmochimical Acta 57, 683–684.

Bodnar, R.J., Vityk, M.O., 1994. Interpretation of microthermometric data for H_2O–NaCl fluid inclusions. In: De Vivo, B., Frezzotti, M.L. (Eds.), Fluid Inclusions in Minerals: Methods and Applications. Virginia Tech., Potignano-Siena, pp. 117–130.

Brigaud, F., Chapman, D.S., Le Douaran, S., 1990. Estimating thermal conductivity in sedimentary basins using lithologic data and geophysical well logs. AAPG Bulletin 74, 1459–1477.

Bruckschen, P., Oesmann, S., Veizer, J., 1999. Isotope stratigraphy of the European Carboniferous: proxy signals for ocean chemistry, climate and tectonics. Chemical Geology 161, 127–163, http://dx.doi.org/10.1016/S0009-2541(99)00084-4.

Bussolotto, M., Benedicto, A., Invernizzi, C., Micarelli, L., Plagnes, V., Deina, G., 2007. Deformation features within an active normal fault zone in carbonate rocks: the Gubbio fault (Central Apennines, Italy). Journal of Structural Geology 29, 2017–2037, http://dx.doi.org/10.1016/j.jsg.2007.07.014.

Chester, J.S., 2003. Mechanical stratigraphy and fault–fold interaction, Absaroka thrust sheet, Salt River Range, Wyoming. Journal of Structural Geology 25, 1171–1192.

Cooke, M.L., Simo, J.A., Underwood, C.A., Rijken, P., 2006. Mechanical stratigraphic controls on fracture patterns within carbonates and implications for groundwater flow. Sedimentary Geology 184, 225–239.

Craddock, J., Van der Pluijm, B.A., 1999. Sevier–Laramide deformation of the continental interior from calcite twinning analysis, west-central North America. Tectonophysics 305, 275–286.

De Keijzer, M., Hillgartner, H., Al Dhahab, S., Rawsley, K., 2007. A sub-surface study of resevoir-scale fracture heterogeneities in Cretaceous carbonates, North Oman. In: Lonergan, L., Jolly, R.J.H., Rawsley, K., Sanderson, D.J. (Eds.), Fractured Reservoirs.Geological Society of London. Special Publication 270, 227–244.

DeCelles, P.G., 1994. Late Cretaceous–Paleocene synorogenic sedimentation and kinematic history of the Sevier thrust belt, northeast Utah and Southwest Wyoming. Geological Society of America Bulletin 106, 36–56.

Dickson, J.A.D., 1966. Carbonate identification and genesis as revealed by staining. Journal of Sedimentary Research 36 (2), 491–505.

Dietrich, D., McKenzie, J.A., Song, H., 1983. Origin of calcite in syntectonic veins as determined from carbon isotopes ratios. Geology 11, 547–551, http://dx.doi.org/10.1130/0091- 7613(1983) 11<547:OOCISV>2.0.CO;2.

Erslev, E.A., 1990. Heterogeneous Laramide deformation in the Rattlesnake Mountain antiticline, Cody, Wyoming. Geologic field tours of western Wyoming and parts of adjacent Idaho, Montana, and Utah. Geological Survey of Wyoming, 29, pp. 141–149.

Erslev, E.A., 1991. Trishear fault-propagation folding. Geology 19, 617–620.

Erslev, E.A., 1995. Heterogeneous Laramide deformation in the Rattlesnake Mountain Anticline, Cody, Wyoming. Field Trip 7, 141–150.

Evans, M.A., Hobbs, G.C., 2003. Fate of 'warm'migrating fluids in the central Appalachians during the Late Paleozoic Alleghanian Orogeny. Journal of Geochemical Exploration 78–79, 327–331, http://dx.doi.org/10.1016/S0375-6742(03)00088-8.

Fischer, M.P., Higuera-Díaz, I.C., Evans, M.A., Perry, E.C., Lefticariu, L., 2009. Fracture-controlled paleohydrology in a map-scale detachment fold: insights from the analysis of fluid inclusions in calcite and quartz veins. Journal of Structural Geology 31, 1490–1510, http://dx.doi.org/10.1016/j.jsg.2009.09.004.

Friedman, I., O'Neil, J.R., 1977. Compilation of stable isotope fractionation factors of geochemical interest. U.S. Geological Survey Professional Paper 440 KK. (12 p.).

Goldstein, R.H., Reynolds, J.T., 1994. Systematics of fluid inclusions in diagenetic minerals Tulsa, Okla Systematics of fluid inclusions in diagenetic mineralsSEPM Short Course 31.

Gross, M.R., 1993. The origin and spacing of cross joints: examples from the Monterey Formation, Santa Barbara Coastline, California. Journal of Structural Geology 15, 737–751.

Gross, M., Fisher, M., Engelder, T., Greenfield, J.R., 1995. Factors controlling joint spacing in interbedded sedimentary rocks: integrating numerical models with field observations from the Monterey Formation, USA. In: Ameen, M.S. (Ed.), Fractography: fracture topography as a tool in fracture mechanics and stress analysis.Geological Society Special Publication 92, 215–233.

Guiton, M., Sassi, W., Leroy, Y., Gauthier, B., 2003. Mechanical constraints on the chronology of fracture activation in the folded Devonian sandstone of the western Moroccan Anti-Atlas. Journal of Structural Geology 25, 1317–1330.
Hanks, C.L., Lorenz, J., Teufel, L., Krumhardt, A.P., 1997. Lithologic and structural controls on natural fracture distribution and behavior within the Lisburne Group, northeastern Brooks Range and North Slope subsurface, Alaska. AAPG Bulletin 81, 1700–1720.
Heasler, H.P., Hinckley, B.S., 1985. Geothermal resources of the Bighorn Basin, Wyoming. The Geological Survey of Wyoming, 8. (27p.).
Hennier, J., Spang, J., 1983. Mechanisms for deformation of sedimentary strata of Sheep Mountain Anticline, Bighorn Basin, Wyoming. Wyoming Geological Association Guidebook, pp. 97–111.
Hennings, P.H., Olson, J.E., Thompson, L.B., 2000. Combining outcrop data and three dimensional structural models to characterize fractured reservoirs: an example from Wyoming. AAPG Bulletin 84, 830–849.
Katz, D., Eberli, G., Swart, P., Smith, L., 2006. Tectonic–Hydrothermal brecciation associated with calcite precipitation and permeability destruction in mississippian carbonate reservoirs, Montana and Wyoming. AAPG Bulletin 90, 1803–1841.
Kluth, C., Coney, P., 1981. Plate tectonics of the Ancestral Rocky Mountains. Geology v9, 10–15.
Kluth, C., Peterson, J., 1986. Plate tectonics of the Ancestral Rocky Mountains. AAPG Memoir 41, 353–368.
Krumgalz, B.S., Pogorelsky, R., Pitzer, K.S., 1996. Volumetric properties of single aqueous electrolytes from zero to saturation concentrations at 298.15 K represented by Pitzer's ion-interaction equation. Journal of Physical and Chemical Reference Data 25, 663–689.
La Pointe, P.R., Hudson, J.A., 1985. Characterization and interpretation of rock mass joint pattern. Geological Society of America Special Paper 199, 37.
Lacombe, O., Bellahsen, N., Mouthereau, F., 2011. Fracture patterns in the Zagros Simply Folded Belt (Fars): new constraints on early collisional tectonic history and role of basement faults. In: Lacombe, O., Grasemann, B., Simpson, G. (Eds.), Geodynamic evolution of the ZagrosGeological Magazine 148, 940–963, http://dx.doi.org/10.1017/S001675681100029X.
Laubach, S.E., Olson, J., Gross, M.R., 2009. Mechanical and fracture stratigraphy. AAPG Bulletin 93, 1413–1427.
Lefticariu, L., Perry, E.C., Fischer, M.P., Banner, J.L., 2005. Evolution of fluid compartmentalization in a detachment fold complex. Geology 33, 69–72, http://dx.doi.org/10.1130/G20592.1.
Lorenz, J.C., Sterling, J.L., Schechter, D.S., Whigham, C.L., Jensen, J.L., 2002. Natural fractures in the Spraberry Formation, Midland Basin, Texas: The effects of mechanical stratigraphy on fracture variability and reservoir behavior. AAPG Bulletin 86, 505–524.
Lynn, H.B., 2004a. The winds of change, anisotropic rocks — their preferred direction of fluid flow and their associated seismic signatures — part 1. The Leading Edge 23, 1156–1162.
Lynn, H.B., 2004b. The winds of change, anisotropic rocks — their preferred direction of fluid flow and their associated seismic signatures — part 2. The Leading Edge 23, 1258–1268.
Machel, H.G., Cavell, P.A., 1999. Low-flux, tectonically-induced squeegee fluid flow ("hot flash") into the Rocky Mountain foreland basin. Bulletin of Canadian Petroleum Geology 47, 510–533.
Machel, H.G., Lonnee, J., 2002. Hydrothermal dolomite — a product of poor definition and imagination. Sedimentary Geology 152, 163–171.
Maughan, E., 1993. The ancestral Rocky Mountains in Wyoming. In: Snoke, A.W., Steidtmann, J.R., Roberts, S.M. (Eds.), Geology of WyomingMemoir: Geological Survey of Wyoming 5, 188–207.
McArthur, J.M., Howarth, R.J., 2004. Strontium isotope stratigraphy. In: Gradstein, F.M., Ogg, J.G., Smith, A.G. (Eds.), A Geologic Time Scale 2004. Cambridge University Press, pp. 96–109.
McLimans, R.K., 1987. The application of fluid inclusions to migration of oil and diagenesis in petroleum reservoirs. In: Hanor, J.S., Kharaka, Y.K., Land, L.S. (Eds.), Conveners, geochemistry of waters in deep sedimentary basins; selected contributions from the Penrose conferenceApplied Geochemistry 2, 585–603.
Mii, H., Grossman, E.L., Yancey, T.E., 1999. Carboniferous isotope stratigraphies of North America: implications for Carboniferous paleoceanography and Mississippian glaciation. Geological Society of America Bulletin 111, 960–973.
Neely, T.G., Erslev, E.A., 2009. The interplay of fold mechanisms and basement weaknesses at the transition between Laramide basement-involved arches, north-central Wyoming, U.S.A. Journal of Structural Geology 31, 1012–1027, http://dx.doi.org/10.1016/j.jsg.2009.03.008.
Olson, J.E., Laubach, S.E., Lander, R.L., 2007. Combining diagenesis and mechanics to quantify fracture aperture distributions and fracture pattern permeability. In: Lonergan, L., Jolley, R.J., Sanderson, D.J., Rawnsley, K. (Eds.), Fractured reservoirs.Geological Society of London. Special Publication 270, 97–112.
Price, N.J., Cosgrove, J.W., 1990. Analysis of Geological Structures. Cambridge University Press, Cambridge. (502 pp.).
Reid, S., Dorobek, S., Loucks, R., Sarg, J., 1993. Sequence stratigraphy and evolution of a progradational, foreland carbonate ramp, Lower Mississippian Mission Canyon Formation and stratigraphic equivalents, Montana and Idaho. AAPG Memoir 57, 327–352.
Rhodes, M.K., Carroll, A.R., Pietras, J.T., Beard, B.L., Johnson, C.M., 2002. Strontium isotope record of paleohydrology and continental weathering, Eocene Green River Formation, Wyoming. Geology 30, 167–170, http://dx.doi.org/10.1130/0091-7613(2002)030<0167:SIROPA>2.0.CO;2.
Rosenbaum, J., Sheppard, S.M.F., 1986. An isotopic study of siderites, dolomites and ankerites at high temperatures. Geochimica et Cosmochimica Acta 50 (6), 1147–1150, http://dx.doi.org/10.1016/0016-7037(86)90396-0.
Royse, F., 1993. An overview of the geologic structure of the thrust belt in Wyoming, northern Utah, and eastern Idaho. In: Snoke, A.W., Steidtmann, J.R., Roberts, S.M. (Eds.), Geology of WyomingMemoir: Geological Survey of Wyoming 5, 272–311.
Sando, W.J., 1988. Madison Limestone (Mississippian) paleokarst: a geologic synthesis. In: James, N.P., Choquette, P.W. (Eds.), Paleokarst. Springer-Verlag, New York, pp. 256–277.
Sanz, P., Pollard, D., Allwardt, P., Borja, R., 2008. Mechanical models of fracture reactivation and slip on bedding surfaces during folding of the asymmetric anticline at Sheep Mountain, Wyoming. Journal of Structural Geology 30, 1177–1191.
Sassi, W., Guiton, M., Leroy, Y.M., Kallel, N., Callot, J.P., Daniel, J.M., Lerat, O., Faure, J.L., 2012. Constraints on mechanical modelling of folding provided by matrix deformation and fracture network analysis: The case of Split Mountain (Utah, USA). Tectonophysics 576-577, 197–215.
Savage, H.M., Cooke, M.L., 2004. The effect of non-parallel thrust fault interaction on fold pattern. Journal of Structural Geology 26, 905–917.
Schneider, F., 2003. basin modeling in complex area: examples from Eastern Venezuelan and Canadian Foothills. Oil and Gas Science and Technology 58 (2), 313–324.
Shackleton, J.R., Cooke, M.L., Sussman, A.J., 2005. Evidence for temporally changing mechanical stratigraphy and effects on vein-network architecture. Geology 33, 101–104.
Smith, B.L., Eberli, G., Sonnenfeld, M.D., 2004. Sequence stratigraphic and paleogeographic distribution of reservoir quality dolomite, Madison Formation, Wyoming and Montana. AAPG Memoir 80, 67–92.
Sonnenfeld, M.D., 1996a. An integrated sequence stratigraphic approach to reservoir characterization of the Lower Mississippian Madison Limestone, emphasizing Elk Basin field, Bighorn Basin, Wyoming. Unpublished PhD dissertation. Colorado School of Mines, Golden, Colorado.
Sonnenfeld, M.D., 1996a. Sequence evolution and hierarchy within the lower Mississippian Madison Limestone of Wyoming. In: Longman, M.W., Sonnenfeld, M.D. (Eds.), Paleozoic Systems of the Rocky Mountain Region. Society for Economic Paleontologists and Mineralogists (Society for Sedimentary Geology) Rocky Mountain Section, pp. 165–192.
Stanton, H., Erslev, E., 2004. Sheep Mountain Anticline: backlimb tightening and sequential deformation in the Bighorn Basin, Wyoming. Wyoming Geological Association Guidebook, 53, pp. 75–87.
Stearns, D.W., 1971. Mechanisms of drape folding in the Wyoming Province, Wyoming. Geological Association Guidebook, 23, pp. 125–144.
Stearns, D., Friedman, M., 1972. Reservoirs in fractured rocks, in stratigraphic oil and gas fields. AAPG Memoir 16, 82–106.
Templeton, A.S., Sweeney, J., Manske, H., Tilghman, J.F., Calhoun, S.C., Voilich, A., Chamberlain, C.P., 1995. Fluids and the Heart Mountain fault revisited. Geology 23, 929–932, http://dx.doi.org/10.1130/0091-7613(1995) 023<0929: FATHMF>2.3.CO;2.
Travé, A., Calvet, F., Sans, M., Vergès, J., Thirlwall, M., 2000. Fluid history related to the Alpine compression at the margin of the south-Pyrenean Foreland basin: the El Guix anticline. Tectonophysics 321, 73–102.
Travé, A., Labaume, P., Vergés, J., 2007. Fluid Systems in foreland fold-and-thrust belts: an overview from the Southern Pyrenees. In: Lacombe, O., Lavé, J., Roure, F., Vergés, J. (Eds.), Thrust Belts and Foreland Basins. Springer, Berlin, pp. 93–115, http://dx.doi.org/10.1007/978-3-540-69426-7_5.
Veizer, J., Ala, D., Azmy, K., Bruckschen, P., Buhl, D., Bruhn, F., Carden, G.A.F., Diener, A., Ebneth, S., Godderis, Y., Jasper, T., Korte, C., Pawellek, F., Podlaha, O.G., Strauss, H., 1999. $^{87}Sr/^{86}Sr$, $\delta^{13}C$ and $\delta^{18}O$ evolution of Phanerozoic seawater. Chemical Geology 161, 59–88, http://dx.doi.org/10.1016/S0009-2541(99)00081-9.
Wachter, E.A., Hayes, J.M., 1985. Exchange of oxygen isotopes in carbon dioxide-phosphoric [correction of phosporic] acid systems. Isotope Geoscience 52, 365–374.
Warren, J.K., 2006. In: Warren, J.K. (Ed.), Evaporites sediments, resources and hydrocarbons. Springer, Berlin Heidelberg.
Wennberg, O.P., Svånå, T., Azizzadeh, M., Aqrawi, A.M.M., Brockbank, P., Lyslo, K.B., Ogilvie, S., 2006. Fracture intensity vs. mechanical stratigraphy in platform top carbonates: the Aquitanian of the Asmari Formation, Khaviz anticline, Zagros, southwest Iran. Petroleum Geoscience 12, 235–246.
Wennberg, O.P., Azizzadeh, M., Aqrawi, A.M., Blanc, E., Brockbank, P., Lyslo, K.B., Pickard, N., Salem, L.D., Svånå, T., 2007. The Khaviz Anticline — an outcrop analogue to giant fractured Asmari Formation reservoirs in SW Iran. In: Jolly, R.J.H., Rawnsley, K., Sanderson, D.J. (Eds.), Fractured Reservoirs.Geological Society of London. Special Publication 270, 23–42.
Westphal, H., Eberli, G., Smith, L.B., Grammer, M., Kislak, J., 2004. Reservoir characterization of the Mississippian Madison Formation, Wind River Basin, Wyoming. AAPG Bulletin 88, 405–432.